

Publications

---

1-17-2023

## Gravity Wave Drag Parameterizations for Earth's Atmosphere

Christopher J. Heale

*Embry-Riddle Aeronautical University, HEALEC@erau.edu*

Christopher G. Kruse

*NorthWest Research Associates*

Jadwiga H. Richter

*National Center for Atmospheric Research*

M. Joan Alexander

*NorthWest Research Associates*

Julio T. Bacmeister

*National Center for Atmospheric Research*

*See next page for additional authors*

Follow this and additional works at: <https://commons.erau.edu/publication>



Part of the [Atmospheric Sciences Commons](#)

---

### Scholarly Commons Citation

Heale, C. J., Kruse, C. G., Richter, J. H., Alexander, M. J., Bacmeister, J. T., & Wei, J. (2023). Gravity Wave Drag Parameterizations for Earth's Atmosphere. *Fast Physics in Large Scale Atmospheric Models: Parameterization, Evaluation, and Observations*, (). <https://doi.org/10.22541/essoar.167397474.46072527/v1>

This Book Chapter is brought to you for free and open access by Scholarly Commons. It has been accepted for inclusion in Publications by an authorized administrator of Scholarly Commons. For more information, please contact [commons@erau.edu](mailto:commons@erau.edu).

---

**Authors**

Christopher J. Heale, Christopher G. Kruse, Jadwiga H. Richter, M. Joan Alexander, Julio T. Bacmeister, and Junhong Wei

# Gravity wave drag parameterizations for Earth’s atmosphere

Christopher G Kruse<sup>1</sup>, Jadwiga H Richter<sup>2</sup>, M. Joan Alexander<sup>1</sup>, Julio T Bacmeister<sup>2</sup>,  
Christopher Heale<sup>3</sup>, and Junhong Wei<sup>4</sup>

<sup>1</sup>NorthWest Research Associates, Boulder, CO, USA

<sup>2</sup>Climate and Global Dynamics Laboratory, National Center for Atmospheric Research,  
Boulder, CO, USA

<sup>3</sup>Department of Physical Sciences, Embry–Riddle Aeronautical University, Daytona Beach,  
Florida, USA

<sup>4</sup>School of Atmospheric Sciences and Guangdong Province Key Laboratory for Climate  
Change and Natural Disaster Studies, Sun Yat-sen University, and Southern Marine  
Science and Engineering Guangdong Laboratory (Zhuhai), Zhuhai, China

January 17, 2023

## Abstract

Atmospheric gravity waves (GWs), or buoyancy waves, transport momentum and energy through Earth’s atmosphere. GWs are important at nearly all levels of the atmosphere, though, the momentum they transport is particularly important in general circulation of the middle and upper atmosphere. Primary sources of atmospheric GWs are flow over mountains, moist convection, and imbalances in jet/frontal systems. Secondary GWs can also be generated as a result of dissipation of a primary GWs. Gravity waves typically have horizontal wavelengths of 10’s to 100’s of kilometers, though, they can have scales of 1’s to 1000’s of kilometers as well. Current effective resolutions of climate models, and even numerical weather prediction models, do not resolve significant portions of the momentum- and energy-flux-carrying GW spectrum, and so parameterizations are necessary to represent under- and unresolved GWs in most current models. Here, an overview of GWs generated by orography, convection, jet/front systems, primary wave breaking, and secondary wave generation is provided. The basic theory of GW generation, propagation, and dissipation relevant to parameterization is presented. Conventionally used GW parameterizations are then reviewed. Lastly, we describe uncertainties and parameter tuning in current parameterizations and discuss known processes that are currently missing.

1                                   **Gravity wave drag parameterizations for Earth’s atmosphere**  
2  
3

4                   Christopher G. Kruse<sup>1</sup>, Jadwiga H. Richter<sup>2</sup>, M. Joan Alexander<sup>1</sup>, Julio T. Bacmeister<sup>2</sup>,  
5                                   Christopher Heale<sup>3</sup>, Junhong Wei<sup>4</sup>  
6  
7

8                                   <sup>1</sup>NorthWest Research Associates, Boulder, CO, USA

9                   <sup>2</sup>Climate and Global Dynamics Laboratory, National Center for Atmospheric Research, Boulder,  
10                                   CO, USA

11                   <sup>3</sup>Department of Physical Sciences, Embry–Riddle Aeronautical University, Daytona Beach,  
12                                   Florida, USA

13                   <sup>4</sup>School of Atmospheric Sciences and Guangdong Province Key Laboratory for Climate Change  
14                                   and Natural Disaster Studies, Sun Yat-sen University, and Southern Marine Science and  
15                                   Engineering Guangdong Laboratory (Zhuhai), Zhuhai, China  
16  
17  
18  
19

20                                   **Chapter 11 of AGU Book entitled:**

21                   “Fast Physics in Large Scale Atmospheric Models: Parameterization, Evaluation, and  
22                                   Observations”,

23                                   Editors: Yangang Liu; Pavlos Kollias; Leo Donner (advisor)  
24  
25  
26  
27

28                                   **Corresponding Author:**

29                                   Christopher G. Kruse, ckruse@nwra.com  
30  
31  
32  
33

34 **Abstract**

35

36 Atmospheric gravity waves (GWs), or buoyancy waves, transport momentum and energy  
37 through Earth's atmosphere. GWs are important at nearly all levels of the atmosphere,  
38 though, the momentum they transport is particularly important in general circulation of the  
39 middle and upper atmosphere. Primary sources of atmospheric GWs are flow over mountains,  
40 moist convection, and imbalances in jet/frontal systems. Secondary GWs can also be generated  
41 as a result of dissipation of a primary GWs. Gravity waves typically have horizontal wavelengths  
42 of 10's to 100's of kilometers, though, they can have scales of 1's to 1000's of kilometers as  
43 well. Current effective resolutions of climate models, and even numerical weather prediction  
44 models, do not resolve significant portions of the momentum- and energy-flux-carrying GW  
45 spectrum, and so parameterizations are necessary to represent under- and unresolved GWs in  
46 most current models. Here, an overview of GWs generated by orography, convection, jet/front  
47 systems, primary wave breaking, and secondary wave generation is provided. The basic theory of  
48 GW generation, propagation, and dissipation relevant to parameterization is presented.  
49 Conventionally used GW parameterizations are then reviewed. Lastly, we describe uncertainties  
50 and parameter tuning in current parameterizations and discuss known processes that are currently  
51 missing.

## 52 11.1 Introduction and basic equations

53

54 Gravity waves (GWs), or buoyancy waves, are waves in Earth's atmosphere for which buoyancy  
55 is the restoring force. Most are familiar with the concentric waves that form on the surface of the  
56 water and emanate away from the perturbation from a falling stone: such waves exist on the  
57 boundary of a denser fluid (water) and less dense air above. Atmospheric GWs are analogous to  
58 surface waves, with the same buoyancy restoring force. However, the atmosphere is  
59 continuously stratified, with a more-or-less smooth decrease in potential density with height. In  
60 the continuously stratified atmosphere, lower-level atmospheric GW perturbations displace the  
61 stably-stratified atmospheric flows above, allowing propagation in the vertical as well as the  
62 horizontal (i.e. in all three dimensions).

63

64 Sources of atmospheric GWs are numerous. Essentially any process, often an instability, that  
65 produces transient perturbations of air parcels (e.g. in their altitude or potential density) can be a  
66 GW source. However, three primary sources are flow over mountains, moist convection, and  
67 imbalances associated with jets and fronts. Recent studies have focused on secondary GWs  
68 generated as a result of localized breaking/dissipation of a primary GW. Gravity waves typically  
69 have horizontal wavelengths of 10's to 100's of kilometers, and vertical scales of 3 to 30 km,  
70 with periods ranging from about 10 min to several hours. Still, GWs, often orographically forced,  
71 with horizontal scales of a few kilometers are not uncommon. Some sources (e.g. jet/front  
72 imbalances) can generate waves with larger horizontal wavelengths, too, with scales of  $\approx 500$  km  
73 and periods between 6 and 24 hours. These waves are typically classified as inertia-gravity  
74 waves, where the Coriolis effect cannot be neglected. The properties of GWs at various levels of  
75 the atmosphere vary dependent on the GW source, altitude, and atmospheric properties that they  
76 have propagated through.

77

78 Numerous review articles (e.g. Smith 1979, Fritts and Alexander 2003, Teixeira 2014) and  
79 textbooks (e.g. Holton 2004) present the basic, and not so basic, theory of atmospheric GWs. For  
80 full derivations and rigorous mathematical treatment, the reader is directed to these references.  
81 Here, basic relations from linear GW theory are presented to demonstrate fundamental ideas  
82 relevant to GW parameterizations.

83

84 Characteristics of GWs are governed by a dispersion relation that gives the relationship between  
85 the wave frequency and its horizontal and vertical wavenumbers. The following dispersion  
86 relation for two-dimensional (i.e.  $x$  and  $z$ ) gravity waves in a non-rotating atmosphere can be  
87 derived from linearized Boussinesq equations of motions (e.g. Holton et al. 2004):

88

$$89 \quad \omega^{*2} = (\omega - Uk)^2 = \frac{N^2 k^2}{(k^2 + m^2)}, \quad (1)$$

90

91 Here,  $\omega^{*2}$  is the intrinsic frequency of the wave, which is the oscillation frequency an air parcel  
92 experiences as it is advected through the wave,  $\omega$  is the wave, or parcel oscillation, frequency  
93 relative to the ground,  $k = 2\pi/\lambda_x$  and  $m = 2\pi/\lambda_z$  are the horizontal and vertical wavenumbers,  
94 respectively,  $U$  is the background wind, and  $N^2 = \frac{g}{\theta} \frac{\partial \theta}{\partial z}$  is the background atmospheric buoyancy  
95 frequency where  $\theta$  is the background potential temperature.

96

(1) can be solved for the vertical wavenumber as follows:

$$m^2 = \frac{k^2(N^2 - \omega^{*2})}{\omega^{*2}} \quad (2)$$

Another key property of gravity waves is the horizontal wave phase speed,  $c_{px}$ :

$$c_{px} = \frac{\omega}{k} \quad (3)$$

The above is the wave phase speed relative to the ground. The intrinsic wave phase speed, or phase speed relative to the mean wind is defined as:

$$c_{px}^* = \frac{\omega^*}{k} = c_{px} - U = \pm \frac{N}{(k^2 + m^2)^{\frac{1}{2}}} \quad (4)$$

The wave phase speed, as will be described in later sections, largely determines whether waves are able to propagate upwards and where they will break and deposit momentum to the mean flow. Horizontal group velocity,  $c_{gx}$ , or the speed of energy propagation, is related to the intrinsic phase speed through:

$$c_{gx} = \frac{\partial \omega}{\partial k} = U + c_{px}^* \quad (5)$$

where

$$c_{px}^* = \frac{\partial \omega^*}{\partial k} = c_{px}^* \left( 1 - \frac{k^2}{k^2 + m^2} \right). \quad (6)$$

For stationary orographic GWs (OGWs), or mountain waves (MWs), the ground-relative phase speed is zero, so the horizontal intrinsic phase speed exactly opposes the background wind (i.e.  $c_{px}^* = -U$  via (4)). In the hydrostatic limit ( $k \ll m$ ), the horizontal group velocity is the same as the horizontal phase speed. This means the horizontal group velocity is zero for hydrostatic OGWs, therefore these OGWs primarily stay over the orography that generated them. However, for  $k \sim m$ , the horizontal group velocity becomes non-zero in the direction of the background flow for non-hydrostatic OGWs, leading to their energy propagation and presence downstream. The speed at which the GW energy propagates in the vertical is described by the vertical group velocity:

$$c_{gz} = \frac{\partial \omega}{\partial m} = \frac{\omega^*}{m} \left( \frac{m^2}{m^2 + k^2} \right) \quad (7)$$

In the hydrostatic limit and using (1) and (3), the vertical group velocity becomes

$$c_{gz} \approx \pm \frac{(c_{px} - U)^2 k}{N}. \quad (8)$$

137 According to (8), the speed at which hydrostatic GWs propagate upward is proportional to the  
 138 squared intrinsic phase speed and inversely proportional to horizontal wavelength and stability.  
 139 For a given environment, GWs with shorter horizontal scales propagate upward more quickly, at  
 140 least until non-hydrostatic effects become important (i.e. when  $k$  becomes comparable to  $m$ ).

141

### 142 11.1.2 Mountain Waves

143

144 MWs are GWs generated by stably-stratified flow over mountains. MWs are perhaps the  
 145 most well-known type of atmospheric GWs, being quite visible, quasi-stationary, and the subject  
 146 of research for at least a century (e.g. Lyra 1940, Smith 2019). MWs typically form above and  
 147 downwind of topographic features. Their presence is often indicated by quasi-stationary  
 148 lenticular clouds visible from the ground and in satellite images. The properties of mountain  
 149 waves are determined by the size and shape of the topography as well as by the vertical profiles  
 150 of wind, temperature, and moisture in the surrounding flow. Linear theory can predict the general  
 151 features of MWs when the mountain height is small in comparison to the vertical wavelength of  
 152 the wave.

153 Conventional linear MW theory assumes MWs are stationary, with zero ground-relative  
 154 horizontal phase speed or frequency ( $c_{px}, \omega = 0$ ). Such MWs have phase lines (e.g. wave crests)  
 155 that tilt upstream with height. The dispersion relation, (2), can be written for stationary waves as:

156

$$157 \quad m^2 = k^2 \left( \frac{N^2 - (Uk)^2}{(Uk)^2} \right). \quad (9)$$

158

159 Solutions of flow over small-scale, sinusoidal ridges, where the intrinsic frequency of these  
 160 parcels is higher than the buoyancy frequency (i.e.  $Uk > N$  and hence  $m$  in (9) is imaginary),  
 161 decay exponentially with height. Flow over wider ridges (for which  $f < Uk < N$ ) generate MWs  
 162 that propagate vertically (Smith 1979, Durran 1986b, Holton 1992).

163

164 Linear theory has also been used successfully to describe the basic properties of mountain  
 165 waves generated by compact, or spatially limited, obstacles (e.g.: Lyra 1940, 1943, Queney 1947,  
 166 Scorer 1949, Smith 1979, Durran 2003). Some non-linear solutions to flow over compact  
 167 obstacles exist as well (e.g. Huppert and Miles 1969), though, here linear theory is the focus.  
 168 Flow over an isolated ridge will generate a horizontal spectrum of waves, and each wave  
 169 component will either propagate upwards or decay depending on its  $m$  derived from (9) for its  $k$ .  
 170 (6) shows that for a 2D flow over a wider ridge, the (hydrostatic) horizontal group velocity is  
 171 close to the horizontal phase speed so wave energy is contained above the mountain only, with  
 172 little propagation downstream of the mountain. However, if the mountain ridge is sufficiently  
 173 narrow, nonhydrostatic waves with downstream group velocity can be generated. If atmospheric  
 174 conditions are such that  $m^2 > 0$  near the surface, but becomes negative further aloft, MWs are  
 175 reflected and a train of trapped lee waves may be generated downstream of the forcing (Scorer  
 176 1949). This can happen, for example, when there is strong positive vertical shear of the wind,  
 177  $U_z > 0$ , or a sharp reduction in  $N$  due to an inversion, over narrow ridges. In three dimensional  
 178 flows over obstacles with finite scales in both horizontal dimensions, oblique modes (those at an  
 179 angle between  $0^\circ$  and  $90^\circ$  to the incident wind) can also propagate downstream, even in the  
 180 hydrostatic limit (Smith 1980, Sato et al. 2012, Jiang et al. 2019). This contributes to the  
 181 appearance of broad, large-amplitude perturbations often seen in satellite data significantly



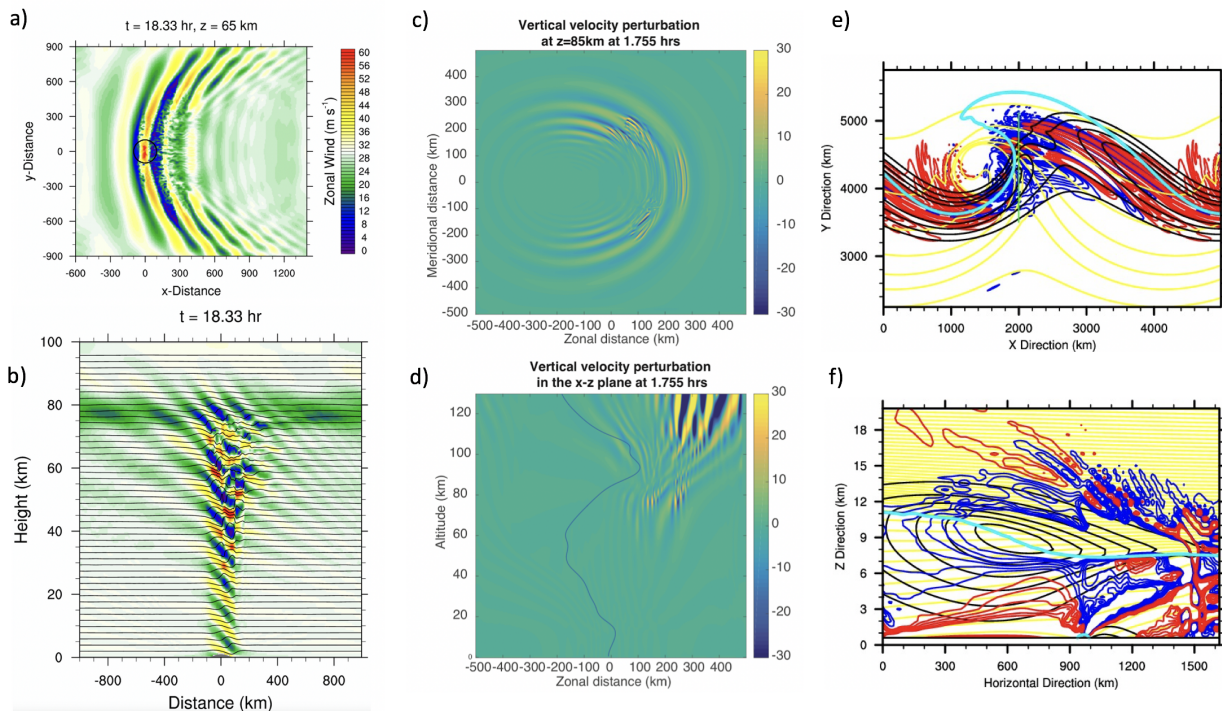
182 downwind of large orographic features such as the Antarctic Peninsula and the terminus of the  
183 Andes (e.g. Alexander et al. 2009, Hoffmann et al. 2013, Hoffmann et al. 2016). High-resolution,  
184 three-dimensional simulations have been critical in developing realistic representations of MW  
185 generation and have shown that three-dimensional dispersion spreads the gravity wave energy,  
186 reducing the amplitude with increasing height relative to only vertically-propagating MWs  
187 (Eckermann et al 2015).

188  
189 In addition to upward propagating mountain waves, flow in a mountainous region can produce  
190 low-level blocking upstream and downslope windstorms downstream. Low-level blocking  
191 occurs when the mean flow does not have enough kinetic energy to traverse an obstacle and  
192 either stops upstream or diverges around the obstacle (Pierrehumbert and Wyman, 1985, Lin and  
193 Wang 1985, Smolarkiewicz and Rotunno 1990, Hughes et al. 2009). Blocking can significantly  
194 impact the waves generated, the orographic drag on the flow, and precipitation patterns. The  
195 Froude number,  $F_r = \frac{U}{Nh_m}$  where  $h_m$  is the height of the mountain, in large part determines  
196 whether blocking will occur (Pierrehumbert and Wyman, 1985, Lin and Wang 1996). When  $F_r >$   
197  $> 1$ , the flow is said to be linear. A flow in this regime has enough kinetic energy to easily  
198 traverse the mountain and dynamic wave amplitudes are small (i.e.  $u' \ll U$ ). When  $F_r \sim 1$ , the  
199 validity of linear theory is questionable and nonlinear terms become important. When  $F_r < 1$ , the  
200 flow is strongly nonlinear and low-level flow may not traverse the mountain, becoming blocked  
201 upstream or diverting around the obstacles (Shepherd 1956, Drazin 1961, Leo et al. 2016). The  
202 evolution of nonlinear low-level flows depends on obstacle aspect ratios (e.g. Miranda and James  
203 1992; Olafsson and Bougeault 1996), orientation, and shape (Phillips 1984). In this situation, the  
204 pressure force by the atmosphere on the orography, and the corresponding drag by the orography  
205 back on the low-level flow in part due to the non-linear blocked flow and in part due to a  
206 vertically-propagating MW response in the atmosphere a bit further aloft. When orographic  
207 blocking occurs, the momentum flux of the vertically-propagating MWs is reduced relative to  
208 what linear theory alone predicts.

209  
210 Downslope wind storms can exist on a downstream side of a mountain, in particular ones with  
211 steep leeside slopes, with wind gusts that can exceed  $50 \text{ m s}^{-1}$  (Clark and Peltier 1977, Lilly  
212 1978, Lilly and Klemp 1979, Peltier and Clark 1979, Smith 1985, Bacmeister and Pierrehumbert  
213 1988, Durran 1990, Durran 1986a). In addition, flow configurations analogous to hydraulic  
214 trans-critical flows (Smith 1985, Durran 1986a) can form leading to significantly enhanced drag  
215 on the low-level flow. These flows are responsible for many of the named downslope winds that  
216 occur around large mountain ranges: e.g. Chinooks, Santa Anas, Föhn, Zondas. Nonlinear two-  
217 dimensional flow over obstacles has been investigated extensively over several decades (e.g.:  
218 Clark and Peltier 1977, Durran and Klemp 1983, Clark and Peltier 1984, Durran and Klemp  
219 1983, Durran 1986a, Durran and Klemp 1987, Bacmeister and Schoeberl 1989, Lott 1998,  
220 Farmer and Armi 1999, Winters and Armi 2014). These studies have led to important insights  
221 about stability, hydraulic analogs, downslope winds, and time-dependence in mountain wave  
222 flows. Results from 3D numerical simulations were used explicitly in developing more complete  
223 orographic gravity wave drag parameterization schemes for global models (e.g. Lott and Miller  
224 1997, Scinocca and McFarlane 2000, Webster et al. 2003).

225  
226 In addition to drag from mesoscale OGWs, another important source of low-level orographic  
227 drag in the atmosphere is turbulent orographic form drag (TOFD). This is drag produced in the

228 boundary layer by small obstacles ( $< 5$  km). In contrast to OGW, this drag is produced in all  
 229 stratification-regimes, but does not carry momentum flux out of the boundary layer (e.g. Beljaars  
 230 et al 2003).  
 231



232

233

234

235 *Figure 1: Depiction of three dominant sources of GWs: a, b) Orographic,*  
 236 *c, d) Convective, and e, f) Frontal. Corresponding animations can be found at:*  
 237 <http://www.cgd.ucar.edu/staff/jrichter/animations.html>

238

239 *a, b): 3D simulation of orographic gravity waves by an 200-km-wide, 1000-m-high isotropic*  
 240 *compact-cosine mountain using the WRF model. (bottom) Zonal winds (color shaded) and*  
 241 *isentropes (contoured) are shown in the x-z slice through the middle of the 3-D domain. (top)*  
 242 *Zonal winds (color shaded) are shown in an x-y slice through  $z = 65$  km. The single contour*  
 243 *shows the spatial extent of the mountain. Both panels are from 18.33 hours after the start of*  
 244 *cross-mountain flow, just after wave breaking has begun. Buoyancy frequency,  $N$ , is  $0.02 s^{-1}$  and*  
 245 *constant environmental zonal mean wind of  $30 m s^{-1}$  was specified. A Rayleigh damping layer*  
 246 *starts at  $z = 70$  km. The WRF setup here is a 3-D extension of that described by Kruse and Smith*  
 247 *(2018).*

248

249 *c, d): 3D simulation of convectively generated gravity waves using the Complex Geometry*  
 250 *Compressible Atmospheric Model (CGCAM) (Felton and Lund, 2006). Latent heating is used as*  
 251 *a proxy for convection. Top panel shows a cross-section at  $z = 85$  km 1.755 hrs into the*  
 252 *simulation, whereas the bottom panel shows a vertical cross-section through the center of the*  
 253 *domain at the same time. Shading indicates vertical velocity perturbations. Solid thin line depicts*  
 254 *the background zonal mean wind profile. Adapted from Heale et al. 2020.*

255

256 *e, f) Gravity waves simulated by a high-resolution idealized weak moist baroclinic wave*  
257 *simulation using the WRF model in Wei and Zhang (2014): (e) The horizontal view of the*  
258 *simulated 1-km temperature (yellow lines; contour interval is 5 K), 7-km dynamic tropopause*  
259 *where potential vorticity equals 1.5 PVU (turquoise lines), 8-km horizontal wind (black lines;*  
260 *contours at 40, 45, 50, and 55 m s<sup>-1</sup>), and 12-km horizontal divergence (blue lines, positive; red*  
261 *lines, negative; contour interval is 2.0\*10<sup>-6</sup> s<sup>-1</sup>; range is between -1.2\*10<sup>-5</sup> s<sup>-1</sup> and 1.2\*10<sup>-5</sup> s<sup>-1</sup>;*  
262 *zero value omitted). (f) The vertical cross section along the green line in (e) for the simulated*  
263 *potential temperature (yellow lines; contour interval is 5 K), dynamic tropopause where*  
264 *potential vorticity equals 1.5 PVU (turquoise lines), horizontal wind (black lines; contours at 30,*  
265 *35, 40, 45, 50, 55, 60 and 65 m s<sup>-1</sup>), and horizontal divergence (blue lines, positive; red lines,*  
266 *negative; contour interval is 2.0\*10<sup>-6</sup> s<sup>-1</sup>; range is between -1.2\*10<sup>-5</sup> s<sup>-1</sup> and 1.2\*10<sup>-5</sup> s<sup>-1</sup>; zero*  
267 *value omitted). Figure courtesy of J. Wei.*  
268  
269

270 Figures 1a, b show the vertical and horizontal properties of mountain waves generated over an  
271 isolated obstacle. In this case, the MWs forced by the topography are linear and approximately  
272 hydrostatic. These hydrostatic waves primarily stay over the idealized mountain below (Fig. 1b).  
273 Wave amplitudes grow with height, resulting in breaking in the upper atmosphere above  $z \sim 60$   
274 km. Figure 1a shows MW perturbations in the horizontal plane at the height of 65 km. Strongest  
275 perturbations are right over the obstacle and show a bow-shaped structure with decaying  
276 amplitudes away from the obstacle in the direction perpendicular to the mean flow. At 65 km in  
277 this particular simulation, gravity wave breaking has already begun.  
278

279 The supplementary Animation 1 (<http://www.cgd.ucar.edu/staff/jrichter/animations.html>) shows  
280 the time evolution of MW generation shown in Figures 1a,b. Gravity waves form almost  
281 immediately over the obstacle and then propagate upwards. Smaller-scale MWs appear first,  
282 within  $\sim 5$  hours, at mesospheric altitudes, consistent with (8). The MW at  $z = 65$  km grows in  
283 amplitude and scale with time, as longer waves build in having had enough time to reach this  
284 altitude. By  $\sim 15$  hours into the simulation, the MW field begins to break, in this case via wave  
285 overturning and static instability as no turbulence parameterization was used. The entire wave  
286 field quickly dissipates after  $\sim 24$  hrs into the simulation, in part due to wave breaking and also  
287 in part due cessation of cross-barrier flow at  $t = 24$  hrs. The complexity of the wave breaking is  
288 well visualized by the right-hand panel of supplementary Animation 1 which shows a horizontal  
289 cross-section through the wind field at 65 km. Up to 15 hrs into the visualization, coherent wave  
290 crest/troughs are present throughout the model domain. After breaking begins, turbulent features  
291 at the grid-scale become apparent and secondary waves are generated, which appear throughout  
292 the doubly-periodic domain. Supplementary Animation 2 shows the characteristics of the gravity  
293 wave field at various altitudes at 18.33 hours into the simulation. The visualization shows largest  
294 wave amplitudes within 200 km from the center of the obstacle in the cross-wind direction, with  
295 waves extending in a quasi V-shape away from the obstacle, if looking in the direction of the  
296 mean wind at the wave field. Hence, most of the perturbations associated with the flow over the  
297 obstacle are directly over the obstacle and in the bow-shaped region downwind and away from  
298 the obstacle. Wave breaking begins at 47 km in this particular simulation, intensifying with  
299 altitude.  
300  
301

### 302 11.1.3 Convectively generated gravity waves

303

304 Moist convection is another prominent source of GWs and the dominant GW source in  
305 the Tropics. Two and three-dimensional numerical simulations of convection reveal that  
306 convection excites a broad spectrum of waves with horizontal wavelengths between 10 and 100's  
307 km, and periods from a few minutes to several hours (e.g.: Alexander et al. 1995, Alexander and  
308 Holton 1997, Piani et al. 2000, Piani and Durran 2001). The vertical wavelengths of  
309 convectively generated gravity waves can vary between several kilometers up to 40 km (e.g.  
310 Alexander and Holton 2004). Convectively generated gravity waves are rarely symmetric in the  
311 horizontal plane, and typically have a preferred propagation direction, which is determined by  
312 the vertical structure of the horizontal wind within which the convection and GW generation  
313 occur (Beres et al. 2002).

314

315 Generation of gravity waves by convection is a complex nonlinear process, but has been  
316 described via three linear mechanisms, all of which are ultimately a response to latent heating:

317

318 1) Thermal or diabatic forcing: in this mechanism temporal and spatial variations of  
319 convective heating produce perturbations in potential density that force a spectrum of  
320 GWs. This mechanism was found to be of primary importance by Bretherton et al 1988,  
321 Lin et al. 1998, Chun and Baik 1998, and Pandya and Alexander (1999). Based on 2-D  
322 linearized governing equations, the dominant characteristics of the spectrum of  
323 convectively generated GWs the generated by thermal forcing are determined by the  
324 vertical scale of the heating region and the horizontal wavenumber and frequency  
325 distribution of the heating (Holton et al. 2002). Beres (2004) has shown that the three-  
326 dimensional wave forcing problem can be treated as a multiple two-dimensional problem,  
327 and the gravity wave spectrum in a given azimuthal direction depends on the heating and  
328 mean wind projection in that direction.

329

330 2) Mechanical oscillator: oscillating updrafts and downdrafts about a level of neutral  
331 buoyancy (LNB) (e.g. the top of the boundary layer, tropopause) perturb the stably-  
332 stratified atmosphere at and above the top of the convective motions. For deep, moist  
333 convection, updrafts often overshoot their LNBs (i.e. the tropopause), potentially forcing  
334 vertically-propagating GWs. Transience in convective updraft strength can perpetuate  
335 this forcing. These oscillations can produce upward propagating waves in a manner  
336 similar to a mechanical oscillator in a stratified fluid (Clark et al. 1986, Fovell et al.  
337 1992). Some studies have found this oscillator mechanism to dominate GW generation  
338 (e.g. Lane et al. 2001), whereas others found thermal and mechanical forcing terms are  
339 both equally important (Song et al. 2003). In the set of nonlinear equations, flux terms  
340 couple the thermodynamic and momentum equations, and the nonlinear momentum term  
341 can oppose the heat source giving some apparent cancellation (Pandya and Alexander  
342 1999, Chun et al. 2008).

343

344 3) Obstacle effect or moving mountain: in this mechanism, the top of a convective element  
345 acts as a barrier to the background mean flow, producing upstream propagating waves in  
346 a manner similar to flow over a mountain (Clark et al. 1986, Pfister et al. 1993). Vertical  
347 wind shear, at least near the tops of the convection, is required for this mechanism. The

348 non-zero net vertically-propagating GW momentum flux is fundamentally derived from  
349 the convective momentum fluxes, as convective updrafts vertically transport air parcels  
350 with low (high) momentum into regions of high (low) above. Waves generated by the  
351 obstacle effect are not stationary relative to the ground as in the case of mountain waves,  
352 but rather have horizontal phase speeds similar to the horizontal speed of the convection.  
353

354 Gravity waves generated by a thermal forcing (proxy for convection) are shown in Figures 1c,d  
355 and supplementary Animation 3. Figure 1c and left panel of Animation 3 show that gravity  
356 waves propagate away from the convective source in nearly concentric circles spreading away  
357 from the source as they propagate upward. In a x-z cross-section (Figure 1d and right panel of  
358 Animation 3), convectively generated gravity waves form a fan-like structure with a broad  
359 spectrum of wave phase speeds, and horizontal and vertical wavelengths. In this particular  
360 simulation, westward propagating waves are not as apparent at  $z = 85$  km, due to much slower  
361 vertical group velocity (8) and dissipation in the stratosphere, resulting in asymmetry in Figure  
362 1c. The eastward propagating waves have higher intrinsic phase speeds in the stratosphere and  
363 lower mesosphere, propagate upward more quickly, and break in the mesopause region where  
364 the mesospheric winds shear brings the environmental winds close to the phase speeds of these  
365 eastward propagating waves (Figure 1d).

#### 366 **11.1.4 Gravity waves generated by fronts and jets**

367  
368  
369 Fronts and jets are another major source of GWs in the atmosphere and a significant source of  
370 GWs in mid-latitudes. GWs from front/jet systems have been observed on numerous occasions  
371 (e.g.: Uccellini and Koch, 1987, Sato et al. 1994, Plougonven et al. 2003, Wang and Geller 2003,  
372 Zhang and Yi, 2005, 2008)) and simulated with numerical models (Zhang and Fritsch 1988,  
373 Schmidt and Cotton 1990, Jin 1997, Powers and Reed 1993, Kaplan et al. 1997, Zhang and  
374 Koch 2000, Zhang et al. 2001, 2003). Jets/fronts generate mesoscale and low-frequency gravity  
375 waves (inertia-gravity waves), for which the rotation of the Earth has an influence and the  
376 frequency is of the order of the Coriolis parameter,  $f$ . Wei and Zhang (2014), for example,  
377 examined gravity waves in moist baroclinic jet–front systems with varying degrees of moisture  
378 and found the gravity waves to have horizontal scales between 50 and 500 km, vertical scales  
379 between 1 to 6 km, and frequencies of 1 to  $15 \times 10^{-4} \text{ s}^{-1}$  (periods of 1 to 17 hrs). Most intense  
380 gravity wave activity has been observed and modeled near the vicinity of the maximum of the jet  
381 velocity (strong curvature of the jet) (Plougonven et al., 2003) and in the exit region of upper-  
382 tropospheric jet streaks (e.g.: Guest et al. 2000, Zhang et al. 2001, 2003, Zhang 2004, Wu and  
383 Zhang 2004).

384  
385 The generation mechanisms of gravity waves generated by jet/front systems are still not well  
386 understood. Plougonven and Zhang (2014) present a complete review of possible generation  
387 mechanisms by such systems. Below, three dry-idealized mechanisms that are thought to be most  
388 important are described, two of which form the basis of gravity wave source parameterizations  
389 described in subsequent sections:

- 390  
391 1) Spontaneous imbalance adjustment (see 3.1 of Plougonven and Zhang 2014):  
392 Spontaneous imbalance adjustment is considered a generalization of geostrophic  
393 adjustment. In this mechanism, GWs are generated and radiated away as some initially

394 imbalanced flow comes back into balance. This concept does not address the cause of the  
395 initial imbalance, but only considers the GW emission during the evolution back toward  
396 some (e.g. geostrophic, cyclogeostrophic) balance. This mechanism is responsible for  
397 emission of large-amplitude inertia-gravity waves in regions of strong horizontal  
398 curvature of the wind where the flow becomes unbalanced (Fritts and Luo 1992, Luo and  
399 Fritts 1993). The residual of the nonlinear balance equation is found to be a useful  
400 quantity in diagnosing regions of flow imbalance and predicting regions of wave  
401 generation (Zhang et al 2000, 2001, Zhang 2004). Readers are also referred to the review  
402 by Ruppert et al. (2021) on this topic.

403  
404 2) Adjustment emission (see 3.2-3.4 of Plougonven and Zhang 2014): in this mechanism  
405 well-balanced flow more continuously radiates GWs during the course of its near-  
406 balanced evolution. An early example of such physics was presented by Lighthill (1952),  
407 where acoustic waves are generated within fluids by turbulent motions. Adjustment  
408 emission has successfully replicated the salient characteristics of gravity waves emitted  
409 from vortices and jets in the shallow water model (e.g., Ford 1994a, Ford 1994b,  
410 Sugimoto et al. 2008) and in a stratified fluid (e.g., Plougonven and Zeitlin 2002;  
411 Schecter 2008). Transient generation in sheared disturbances describes how the evolution  
412 of potential vorticity anomalies in a sheared flow leads to a transient generation of gravity  
413 waves, which has been discussed in horizontal (Vanneste and Yavneh 2004) and vertical  
414 shear (Lott et al. 2010).

415 3) Shear instability: in this mechanism gravity wave emission occurs via nonlinear  
416 interaction between Kelvin-Helmholtz instability and propagating modes (Bühler et al.  
417 1999, Scinocca and Ford 2000). Shear instability is usually considered by neglecting the  
418 Coriolis effect. This mechanism of wave generation can occur in very intense shear layers  
419 near the surface or at upper levels, above tropopause jets. Kelvin-Helmholtz instability  
420 occurs on very small scales (hundreds of meters in the vertical and tens of kilometers in  
421 the horizontal), hence in order for gravity waves to propagate upwards, nonlinear  
422 emission on the envelope scale (i.e. scale characterizing the extent of K-H instabilities  
423 and mean-flow influence) must occur (Fritts 1984, Chimonas and Grant 1984).

424  
425 Convection often occurs in association with a frontal system and can provide an  
426 additional source of GWs and/or influence the generation of GWs by frontal/jet system. Many  
427 earlier studies of GWs generated by fronts focused on dry idealized baroclinic wave simulations  
428 (e.g., Zhang 2004), however the role of moisture can potentially be very important (Powers  
429 1997, Zhang et al. 2001, Lane and Reeder 2001). Complementary to the work of Zhang (2004),  
430 Wei and Zhang (2014), using cloud permitting mesoscale baroclinic system simulations, showed  
431 that moisture enhances GW amplitudes and generates additional wave modes in comparison with  
432 a dry simulation. Furthermore, based on the study of GWs spectral characteristics using  
433 multidimensional discrete Fourier transforms, Wei et al. (2016) further demonstrated that the dry  
434 jet/front GW source generates a relatively narrow and less symmetric power spectrum centered  
435 around lower phase speeds and horizontal wavenumbers, whereas the moist gravity wave source  
436 generates a broader and more symmetrical power spectrum, with a broader range of phase speeds  
437 and horizontal wavenumbers. Generation of GWs in frontal systems with a lot of moisture is still  
438 a subject of recent research, and diabatic forcing could be a more important generation  
439 mechanism. The role of moisture in producing significant momentum fluxes from front/jet

440 systems has been emphasized by many studies (e.g., Plougonven et al. 2015; Wei et al. 2016;  
441 Holt et al. 2017).

442  
443 GWs generated by idealized weak moist baroclinic jet-front systems are illustrated in Figure 1e,f  
444 and supplementary Animation 4. As the upper level baroclinic jet develops, with an  
445 accompanying deepening surface cyclone, the lower stratospheric (12-km altitude) flow shows a  
446 well-recognized pattern of convergence upstream of the trough and divergence downstream of  
447 the trough (Figure 1e, and left panel of Animation 4). GW generation begins first with weak  
448 amplitude mesoscale GWs appearing in the jet entrance region upstream of the upper level  
449 trough, along the surface warm front. As the system matures, mesoscale GW generation occurs  
450 primarily in the jet exit region, downstream of the trough and above the surface frontal system  
451 (Figure 1f, right panel of Animation 4). In addition, based on a series of four-dimensional ray-  
452 tracing experiments, Wei and Zhang (2015) investigated the propagating wave characteristics  
453 and the potential source mechanisms of several identified lower-stratospheric GWs in this  
454 particular idealized simulation. It was further demonstrated that moist convection may force new  
455 wave modes, modify/enhance the existing dry jet/front wave modes through latent heat release,  
456 and/or modify the new/existing waves through modification of large-scale flow.

457

458

#### 459 **11.1.5: Secondary wave generation**

460

461 An understudied aspect of the GW lifecycle and a likely underestimated GW source is secondary  
462 wave generation (e.g. Bacmeister and Schoeberl 1989), which is generation of GWs by the  
463 momentum deposition of a dissipating primary GW. While the research on secondary GW  
464 generation, propagation, dissipation, and impact is relatively nascent, there is a growing body of  
465 literature on the topic. Currently, at least two secondary GW generations mechanisms have been  
466 explored:

467

468 1) Large-scale secondary GW generation by localized momentum deposition, or body  
469 forces, resulting from a primary GW. The body forcing and secondary GW generation  
470 occurs at scales larger than the horizontal scales of primary GW activity. The body  
471 forcing from these primary GWs can be both dissipative (e.g. where small-scale  
472 instabilities dissipate the wave) and non-dissipative (e.g. a sometimes reversible forcing  
473 on a layer as a GW transiently propagates into and out of it). The latter effect is  
474 sometimes referred to as “self-acceleration” (e.g. Fritts and Dunkerton 1984). Dissipative  
475 secondary GW generation is the focus of Vadas et al. (2003) and Vadas et al. (2018).  
476 Wilhelm et al (2018) has investigated the non-dissipative, resonant radiation of mesoscale  
477 inertia-gravity waves by a horizontally as well as vertically confined submesoscale  
478 gravity wave packet that propagates vertically. It is known from long-short-wave  
479 interaction theory (Tabaei and Akylas 2007; Van den Bremer and Sutherland 2014) that  
480 such a packet of small-scale waves is able to generate a mean flow consisting of  
481 mesoscale wave structures connected to a resonance mechanism, wherein the vertical  
482 phase velocity of the emitted long waves match the vertical group velocity of the small-  
483 scale gravity wave packet, which acts as a traveling wave source.

484

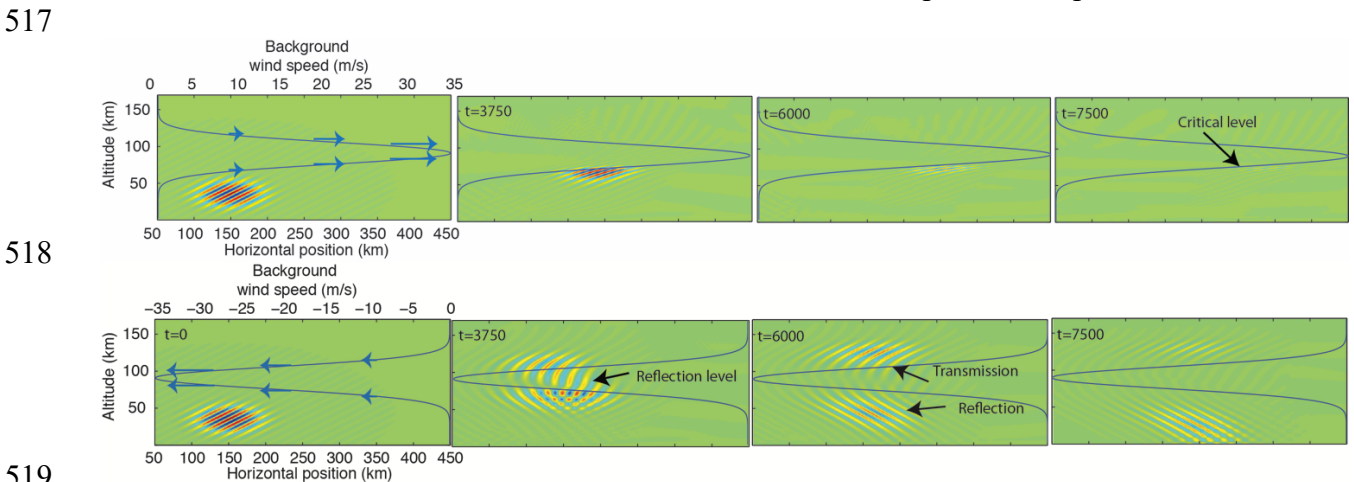


485 2) Secondary GWs are also generated on scales smaller than the horizontal scales of the  
 486 primary GW activity. Numerous small-scale instabilities can take place during GW  
 487 breaking and dissipation. Non-linear dynamics can transfer energy from these small-scale  
 488 instabilities to larger scales that can force a propagating GW (Franke and Robinson  
 489 1999). Instabilities can occur inhomogeneously within a wave field (e.g. in particular  
 490 phases where stratification is reduced, or unstable, where wind shear is increased), also  
 491 forcing waves at scales smaller than wave field (Satomura and Sato 1999, Holton and  
 492 Alexander 1999, Lane and Sharman 2006, Fritts et al. 2006, Chun and Kim 2008, Heale  
 493 et al. 2017, Bossert et al. 2018).

495 At this time, the understanding of secondary GWs is limited; their contribution to the energy and  
 496 momentum budget of the atmosphere is not well understood, nor represented in weather and  
 497 climate models that do not resolve the relevant mechanisms.

498  
 499  
 500 **11.1.6: Gravity wave propagation and dissipation**

501  
 502 GW characteristics change as they propagate through an atmosphere with changing  
 503 buoyancy frequency and mean wind, as suggested by (2). As a GW propagates upward through  
 504 wind shear that is opposite to the wave's propagation direction, the vertical wavelength of the  
 505 wave will increase. Similarly, the vertical wavelength of the wave will decrease when the wave  
 506 propagates through wind shear in the same direction as the wave propagation. If wind in the  
 507 direction of the wave propagation changes so that  $\omega^* = \omega - Uk$  reaches zero, a 'critical level' is  
 508 reached. This is the level at which the horizontal phase speed,  $c_x$ , matches the background wind.  
 509 As a GW approaches a critical level, linear theory predicts the wave vertical wavelength goes to  
 510 zero, zonal wind perturbations go to infinity, and the wave steepens and overturns. Prior to  
 511 reaching the critical level, however, instabilities (e.g. K-H, static instability) are typically  
 512 triggered that dissipate the wave, ending its vertical propagation. This is illustrated in the top  
 513 panel of Figure 2, which shows a wave packet propagating upward and in the positive x direction  
 514 into a region of increasing zonal mean wind (in the same direction as the wave propagation). As  
 515 the wave packet propagates upward, its vertical wavelength decreases as it approaches the  
 516 critical level near  $t = 7500$  and altitude of  $\sim 75$  km, and the GW packet dissipates.





521 **Figure 2:** Simulated propagation of a gravity wave packet through two different  
522 vertically varying background winds (top and bottom) at four different times (from left to right)  
523 using the MAGIC model (Snively and Pasko 2008). The top panel shows a packet propagating in  
524 the same direction as the background wind flow (indicated by the black line), which approaches  
525 a critical level at  $\sim 80$ km and is then absorbed into the mean flow. The bottom panel shows the  
526 same packet propagating against the background wind flow. In this case, the wave encounters a  
527 turning point (reflection) level and partial transmission and reflection occur. The color indicates  
528 the perturbation horizontal wind associated with the gravity wave packet. Times of the  
529 simulation in seconds is depicted in top left corner of the panels. Adapted from Heale and  
530 Snively (2015).

531  
532 When such a wave packet propagates into a region where the wind speed through the  
533 wave increases, the intrinsic phase speed and frequency both increase. According to (2), the  
534 wave packet can reach a level where the intrinsic frequency matches the environmental  
535 buoyancy frequency and the vertical wavelength approaches infinity. This level is referred to as a  
536 turning or reflection level, as at least partial GW reflection occurs here. Above the reflection  
537 level,  $m$  is imaginary and wave evanesces, or decays, exponentially with height. This situation is  
538 illustrated in the bottom row of Figure 2. Where a wave packet is propagating upward and in the  
539 positive  $x$  direction with shear against the direction of propagation above the wave. As the wave  
540 packet approaches the reflection level, the phase lines become more vertically oriented. At  $t =$   
541  $3750$  s, both upward and downward portions of the wave packet superpose to produce the wave  
542 field below the reflection level. Above the reflection level, nearly vertical phase lines are seen,  
543 with a portion of the wave perturbations decaying with height. The wave does not decay above  
544 the reflection level immediately. In this case, the wave maintains enough amplitude to “tunnel”  
545 through this evanescent layer into the slower winds aloft that allow vertical propagation once  
546 again (e.g. Mixa et al. 2021). In this case, part of the wave packet was reflected at the reflection  
547 level, while part was able to tunnel through the evanescent layer and continue propagating  
548 upward.

549  
550 Another important characteristic of GWs is how their amplitudes grow with height, even in an  
551 environment that is constant in height. Linear, 2-D GWs in a horizontally uniform background  
552 have a constant vertical flux of horizontal momentum (e.g.  $\overline{\rho u'w'}$ ) with height (e.g. Eliassen and  
553 Palm 1960). As density decreases exponentially with height, this requires the GW perturbations  
554 to grow exponentially with height. Similar to encountering a critical level, eventually, wave  
555 amplitudes become large and trigger instabilities that dissipate the wave.

### 556 557 **11.1.6: Gravity wave impacts**

558  
559 Both energy and momentum are extracted from the mean flow, or via interaction with  
560 topography, when GWs are generated. Propagating GWs transport this energy and momentum,  
561 depositing them wherever the waves are dissipated. While both are important, the energy  
562 extracted, transported, and deposited is typically neglected. The momentum, however, is not  
563 neglected and represents an important forcing on the background horizontal flow.

564  
565 MWs attain their momentum flux and drag through interactions with orography. Vertically-  
566 propagating MWs induce positive pressure perturbations upstream of the mountains and negative

567 perturbations downstream during generation, resulting in a net horizontal pressure force by the  
 568 atmosphere on the mountains. The mountains exert an equal and opposite force on a lowest layer  
 569 of the atmosphere. This low-level layer then perturbs a layer immediately above and a pressure  
 570 drag by the layer above is exerted on this low-level layer. If no MW dissipation occurs, the  
 571 forces by the mountain and the layer above on the low-level layer cancel, resulting in no net  
 572 horizontal force on this layer. Layers increasingly perturb layers above, propagating the MW  
 573 upward and fluxing atmospheric momentum downward. When the MW dissipates, the top of the  
 574 dissipation layer is no longer displaced by the primary MW. Atmospheric momentum above the  
 575 dissipation layer no longer balances the momentum fluxed out the bottom of this layer, and a net  
 576 force is exerted on the flow. In short, MW drag is exerted wherever the MW is dissipated is  
 577 fundamentally a reaction to pressure forces by the atmosphere on mountains.

578  
 579 While the forcing exerted by non-orographic GW dissipation technically comes out of thin air, it  
 580 does come from somewhere. In general, non-orographic GWs attain the momentum and energy  
 581 they flux from the flow in which they were generated and then spatially redistribute the energy  
 582 and momentum within the atmosphere. Wave fields generated by non-orographic GW fields tend  
 583 to be more complex than MWs, having both a spectrum of spatial scales and a spectrum of phase  
 584 speeds and intrinsic frequencies. For example, in the absence of environmental shear, GWs  
 585 radiate away from moist convection symmetrically in all directions. While the eastward-,  
 586 westward-, northward-, and southward-propagating GWs all flux momentum, the net vertical  
 587 flux of zonal and meridional momentum by these GW beams cancel, resulting in net zero  
 588 momentum flux. While the net momentum fluxes are zero at the source level, wind shear aloft  
 589 forces the different beams of GWs to encounter critical levels at different altitudes and exert  
 590 forces on flows in different directions at different altitudes. Such a phase speed spectrum is  
 591 critically important in forcing the quasi-biennial oscillation and semi-annual oscillation in the  
 592 tropical stratosphere.

593  
 594 While the previous discussion suggests convective GWs are symmetric, they rarely are in reality,  
 595 having a preferred propagation direction and a net momentum flux due to the fact that  
 596 convection often occurs in environments with shear. Wind shear both allows there to be flow  
 597 relative to the tops of the convection and allows convection to transport low-momentum air from  
 598 low lower-levels and act as a barrier to the flow across the top of convection. The convective  
 599 momentum fluxes are likely important in determining a portion of the convective GW spectrum.

600  
 601 GWs generated by jets and fronts derive the energy and momentum they flux from the various  
 602 imbalances that are produced as the systems evolve in time. The GWs are generated by these  
 603 imbalances and adjust the flow in the direction of balance.

604  
 605 Quantitatively, the influence by GWs on the zonal momentum appears when deriving an  
 606 equation for a background or, traditionally, a Reynolds-averaged horizontal wind. These  
 607 equations that govern a larger-scale horizontal flow contain the following term, representing the  
 608 influence of the vertical convergence of the vertical flux of horizontal momentum on the  
 609 background horizontal flow:

610  
 611 
$$GWD = \frac{1}{\bar{\rho}} \frac{\partial}{\partial z} (\bar{\rho} \overline{u'w'}, \bar{\rho} \overline{v'w'}) \quad (10)$$

612  
613 Where  $\bar{\rho}$  is the background atmospheric density,  $u'$ ,  $v'$ , and  $w'$  are the horizontal and vertical  
614 perturbation velocities, and the overline operator,  $\overline{(\cdot)}$ , is a linear background operator of some  
615 kind (e.g. a low-pass filter) used to define the background flow. This term is defined as GW drag  
616 (GWD) and has units of acceleration or drag force per unit mass. While momentum fluxes and  
617 their divergences are obviously relevant to forcing of the background momentum,  
618 pseudomomentum is more relevant to GW dynamics, and its divergence is sometimes used to  
619 quantify GW influences on the mean flow (see Wei et al. 2019 for a comparison of these  
620 approaches).

621  
622 The momentum fluxed and deposited by GWs is significant in Earth's general circulation,  
623 especially in the stratosphere, mesosphere and lower thermosphere. Since GWs grow in  
624 amplitude with height, and background horizontal momentum (e.g.  $\bar{\rho}\bar{u}$ ) decreases with height,  
625 the importance of GWs in the general circulation tends to increase with height. In the lower- to  
626 mid-troposphere, GWs have less influence on large-scale momentum but are still important in  
627 initiating convection and convective organization (Bretherton and Smolarkiewicz 1989, Pandya  
628 and Durran 1996, Shige and Satomura 2000, Lac et al. 2002, Fovell et al. 2006, Lane and Zhang  
629 2011, Su and Zhai 2017, Ruppert et al. 2021). In the upper troposphere and lower stratosphere,  
630 GWD does become important in the zonal mean climate (Palmer et al. 1986, Bacmeister 1993,  
631 Butchart et al. 1998). In the tropical stratosphere, gravity waves contribute 50 to 90% of the  
632 forcing of the Quasi-biennial Oscillation (QBO) (Kawatani et al. 2010, Alexander and Ortland  
633 2010, Richter et al. 2014, Geller et al. 2016, Bushell et al. 2020). In climate models, GW  
634 parameterizations largely determine the period and frequency of the QBO, and most models  
635 without a gravity wave parameterization won't be able to produce a QBO (Giorgetta et al. 2006,  
636 Richter et al. 2014, Geller et al. 2016, Butchart et al. 2018). The representation of the QBO in  
637 climate models is becoming more important as impacts of the QBO on the tropospheric  
638 variability are becoming clearer (Giorgetta et al. 1999, Yoo and Son 2016, Wang et al. 2018).  
639 GWs also contribute to the driving of the semi-annual oscillation (SAO) (Hitchman and Leovy  
640 1988, Ray et al. 1988, Richter and Garcia 2006) and the Mesospheric Semi-Annual Oscillation  
641 (MSAO) (Dunkerton, 1982).

642  
643 In the extratropical stratosphere, GWs provide a portion of the driving of the Brewer Dobson  
644 circulation, especially during the spring-to-summer transition season in each hemisphere  
645 (Alexander and Rosenlof 1996, Rosenlof 1996, Alexander and Rosenlof 2003, Okamoto et al.  
646 2011, de la Camara et al. 2016). MW drag peaks in the upper stratosphere and mesosphere, (e.g.  
647 Kruse 2020), and together with other extratropical GWs, largely from fronts and jets, control the  
648 state of the polar stratospheric temperatures and strength of stratospheric polar night jet, (Boville  
649 1991, Garcia and Boville, 1994). Inadequate representation of GW drag in general circulation  
650 models can lead to a cold bias of southern winter stratosphere temperature in the polar region  
651 (e.g.: Austin et al. 2003, Eyring et al. 2007, McLandress et al. 2012). One of the largest effects  
652 that GWs have on the atmosphere occurs in the mesosphere. Non-orographic GWs dominate GW  
653 drag here and deposit net westward momentum in the winter mesosphere and net eastward  
654 momentum in the summer hemisphere causing the reversal of the zonal mean jets and driving a  
655 mean transport circulation from the summer to winter hemisphere, leading to a warm winter and  
656 cold summer mesopause (Lindzen 1981, Holton 1982, 1983, Garcia and Solomon 1985).  
657

658 Waves that are not filtered by critical levels, reflected by turning levels, and do not break in the  
659 middle atmosphere will be dissipated in the thermosphere by increasing molecular viscosity and  
660 thermal conductivity or, in polar regions, ion drag. The damping rate is inversely proportional to  
661 the vertical wavelength (Walterscheid and Hickey 2011) so waves with larger vertical  
662 wavelengths (and phase speeds) can propagate higher into the thermosphere before dissipating  
663 (Vadas and Fritts 2005, Vadas 2007, Vadas and Nicholls 2012, Heale et al. 2014, 2018).  
664 However, spectra of wave packets that propagate into the thermosphere from below often evolve  
665 from longer to shorter vertical wavelengths in time as a result of dispersion. This occurs because  
666 the longer, faster vertical wavelength components reach the thermosphere, and are dissipated  
667 first, while the shorter, slower components arrive later (Heale et al. 2014, 2018). The dissipation  
668 of these waves produces local body forcing and heating/cooling of the thermosphere (Miyoshi et  
669 al. 2014, Yiğit and Medvedev 2009, Yiğit et al. 2009, Vadas et al. 2014, Hickey et al. 2011) and  
670 will also generate secondary waves (Vadas et al. 2018). It is suggested that wave dissipation in  
671 the thermosphere leads to a drag that opposes the mean zonal winds and is stronger at high  
672 latitudes (Miyoshi et al. 2014) and in the winter hemisphere (Yiğit et al. 2009). Thermospheric  
673 dissipation of waves from deep convective sources can also lead to in-situ generation of  
674 planetary-scale diurnal and semidiurnal tides (Vadas et al. 2014). Waves that reach the  
675 thermosphere can also couple to the ionosphere, producing travelling ionospheric disturbances  
676 (e.g. Liu and Vadas 2013, Azeem et al. 2017, Yu et al. 2017) and ion outflow (Burleigh et al.  
677 2018). Compared to other regions of the atmosphere, the impacts of waves in the thermosphere  
678 are still unknown and require further investigation.

679

680

## 681 **11.2 Representation in large scale models**

682

### 683 **11.2.1 History and basic components**

684

685 The need for representing GWs in General Circulation Models (GCMs) began with the  
686 recognition of ‘missing drag’ in such models. Without explicit drag in the middle atmosphere, if  
687 the atmosphere was in radiative equilibrium, the polar night jet in the stratosphere in models  
688 would be much stronger than observed and the winter (summer) mesopause would not be warm  
689 (cold). Early GCMs which extended to the stratosphere and mesosphere often used Rayleigh  
690 friction to provide a crude parameterization of the effect of breaking gravity waves in the  
691 mesosphere and were able to reproduce the observed features of the zonal mean wind and  
692 temperature in the stratosphere and mesosphere (e.g.: Boville 1986). First implementations of  
693 GW parameterizations in GCMs focused on representing GWs generated by orography (Boer et  
694 al. 1984, Palmer et al 1986, McFarlane 1987). Subsequently, parameterizations in GCMs were  
695 extended to include representation of non-orographic GWs (Rind et al. 1988, Fritts and Lu 1993,  
696 Medvedev and Klaasen 1995, Hines 1997a,b, Alexander and Dunkerton, 1999, Warner and  
697 McIntyre 2001).

698

699 GW parameterizations in GCMs have three basic components: (1) specification of waves at the  
700 source levels, (2) wave propagation with height, and (3) wave dissipation, from which  
701 momentum deposition to the mean flow is estimated. Parameterization of MWs is traditionally  
702 distinguished from non-orographic GWs, with the horizontal phase speed of orographic MWs  
703 assumed to be zero, while non-orographic GWs have a spectrum of phase speeds. Hence, MW

704 drag has historically been treated separately, and this distinction generally remains today. The  
705 source spectra of non-orographic waves initially were specified to be uniform in space and time  
706 in the first implementations of parameterizations in GCMs. Spatially-uniform sources continue to  
707 be standard practice in many GCMs (e.g.: Scinocca et al. 2008, Adachi et al. 2013, Davini et al.  
708 2018). However, in recent years, separate source spectrum parameterizations have been  
709 developed for waves generated by convection and fronts, and these are described in section  
710 12.2.3. These source spectra parameterizations replace the arbitrary/globally defined non-  
711 orographic source spectra in GW parameterizations even though they still carry large  
712 uncertainties.

713

### 714 **11.2.2 Description of GW Parameterizations**

715

716 The primary function of GW parameterizations as currently applied in global models is to  
717 compute the wave-driven force on the mean flow. The mean flow in this context is the grid-box  
718 mean, and the waves are meant to represent sub-grid, or otherwise unresolved, GW anomalies.  
719 The essential ingredients of GW parameterizations include specification of input parameters  
720 describing the gravity wave sources, estimation of the wave dissipation as a function of height,  
721 and output vertical profile of the vector momentum forcing via (10). The wave dissipation profile  
722 implies an energy dissipation rate profile and, in some models (e.g. the Whole Atmosphere  
723 Community Climate Model, Gettleman et al. (2019)), this energy dissipation is tied to vertical  
724 mixing of trace gases. Conversion of energy dissipation to vertical mixing is not direct, however,  
725 because the mixing may be more or less perpendicular to isentrope and tracer gradients (Lelong  
726 and Dunkerton 1998) and so must be scaled by an uncertain Prandtl number, with values  $O(1-100)$   
727 (Smith and Brasseur 1991).

728 GW parameterizations typically start with some specification of the wave stress or momentum  
729 flux along with the wave propagation properties (wavenumbers, phase speeds, propagation  
730 directions) at a source level, which is selected to be somewhere between the surface and the 90  
731 hPa (e.g. near the terrain for MWs and upper troposphere and lower stratosphere for non-  
732 orographic GWs). The vast majority of GW parameterizations assume GWs propagate only  
733 vertically and instantaneously through the column of atmosphere above the source level. Two  
734 notable exceptions are Amemiya and Sato (2010), where 3-D GW propagation was accounted  
735 for, and Eckermann et al. 2015b, which accounted for lateral spreading of MW activity and how  
736 this influenced MW amplitude and breaking levels. Wave dissipation is estimated with a variety  
737 of techniques depending on the parameterization. The plane wave assumption is always made,  
738 so the flux and force both lie along a specified direction of wave propagation. This direction is  
739 specified at the wave source level and is assumed to remain constant through the column until  
740 the wave is completely absorbed. Thus, gravity wave parameterizations are one-dimensional  
741 (vertical), utilizing parameters and model fields that are projected along the direction of wave  
742 propagation. The output force is applied to the vector momentum equations by projection onto  
743 zonal and meridional directions.

744

745 Differences among parameterizations include (a) specification of the sources, and (b)  
746 assumptions that control the wave dissipation with height. For dissipation, Lindzen's (1981)  
747 saturation theory, with modifications formulated by Holton (1982), forms a starting point for  
748 most parameterizations currently in use. Here, parameterized waves are treated as individual  
749 steady hydrostatic monochromatic plane waves. Using (2), the continuity polarization relation

750 ( $k\hat{u} = -m\hat{w}$ ), and the fact that momentum flux for such idealized plane waves is constant in  
 751 height, the following non-dimensional wave amplitude, which quantifies both non-linearity and  
 752 wave steepness, can be derived:

753  
 754

$$755 \quad \frac{\hat{u}}{|U-c|} = \left( \frac{2 MF_{src} N}{\bar{\rho}|U-c_{px}|^3 k} \right)^{\frac{1}{2}} \quad (11)$$

756

757 where hatted quantities are the sinusoidal amplitudes. Here  $MF_{src}$ ,  $k$ , and  $c_{px}$  are constant in  
 758 height. Changes to this non-dimensional GW amplitude in height result from changes in  $\bar{\rho}$ ,  $N$ ,  
 759 and  $|c_{px}^*| = |U - c_{px}|$ . When this non-dimensional amplitude is small, the GW is linear and the  
 760 steepness of the wave, as predicted by this linear theory, is low. As a GW propagates upward,  
 761 density decreases exponentially, and so wave amplitude increases exponentially. Increased  
 762 stratification and environmental wind shear that brings the wind closer to the phase speed can  
 763 both force GW non-linearity.

764

765 When the non-dimensional amplitude, (11), exceeds unity, linear theory predicts the wave will  
 766 loft dense fluid over light fluid and induce static instability. The saturation hypothesis (Lindzen  
 767 1981) assumes instabilities (e.g. static, Kelvin-Helmholtz instabilities) continuously and  
 768 instantaneously prevent the GW from exceeding some non-dimensional wave amplitude (e.g.  
 769 unity for static instability). For example, if a GW is propagating upward in shear that brings the  
 770 environment closer to its phase speed (i.e. as it approaches a critical level), the wave amplitude  
 771 grows. Eventually, this critical wave amplitude is reached. Then, the momentum fluxed by the  
 772 GW is reduced such that (11) gives the critical non-dimensional wave amplitude. The  
 773 momentum flux is reduced with height when the wave is saturated, the vertical derivative of  
 774 which gives the forcing to the mean flow. If the wind shear reverses so that the intrinsic  
 775 frequency increases and the non-dimensional GW amplitude is reduced below the critical  
 776 amplitude, then the GW once again propagates upward conserving its momentum flux and  
 777 exerting no force on the mean flow.

778

779 Other parameterizations in use in global climate models today make different wave dissipation  
 780 assumptions. Alexander and Dunkerton (1999) represent a finely-resolved spectrum of discrete,  
 781 independently treated, monochromatic waves and assumes complete annihilation of an individual  
 782 wave at its breaking level (Alexander and Dunkerton 1999). Hines (1997a,b) proposed a  
 783 “Doppler Spread” mechanism, assuming that nonlinear interactions among waves in the  
 784 spectrum reshape the spectrum with altitude. (See McLandress 1998 for a concise summary of  
 785 the application of the Hines (1997a,b) parameterization.) Warner and McIntyre (2001) assumes  
 786 a similar reshaping of the spectrum with altitude but based on the empirical observations of the  
 787 shape, coupled to Lindzen’s wave saturation concept. Both the Hines and the Warner and  
 788 McIntyre approaches assume a particular vertical wavenumber spectrum shape at the source  
 789 level. A more in-depth overview of such spectral parameterizations not using the conventional  
 790 saturation concept above is provided in Medvedev and Yiğit (2019).

791

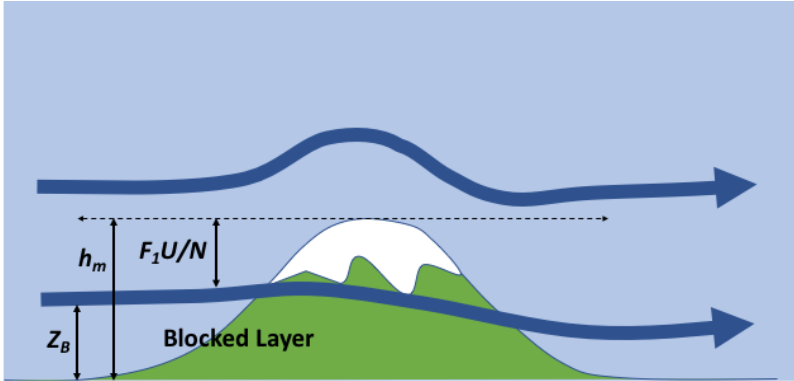
### 792 **11.2.3 GW Source Parameterizations**

793

794 **11.2.3.1 Orography**

795  
796  
797  
798  
799  
800  
801  
802  
803  
804  
805

Specification of MW sources is rather simple in most GCMs. The first formulations prescribed only a single, monochromatic vertically propagating wave with zero horizontal phase speed (Boer et. al 1984, Palmer et al. 1986, and McFarlane 1987), and these formulations are still being used in most GCMs. The GW source specifications are based on 2D theory assuming hydrostatic, steady, horizontally uniform flow over an obstacle. Wave amplitudes at the source levels are defined based on a measure of subgrid-scale orographic variance. In early orographic GW parameterizations, the surface stress vector is parallel to and opposite of the mean flow at the lowest level of the model, assuming isotropic unresolved topography.



806  
807  
808  
809  
810

**Figure 3:** Schematic depiction of flow over and around a large mountain following Lott and Miller (1997).  $h_m$  is the height of the mountain,  $Z_B$  is the height of the blocked layer. Blocked flow can develop if the mountain height exceeds  $F_1(U/N)$ (see text).

811 The first orographic gravity wave drag schemes (e.g. Palmer 1986, McFarlane 1987) neglected the impact of topographic anisotropy and did not consider drag produced by nonlinear dynamics near the surface (e.g. downslope winds, blocking, flow splitting), which can lead to large amplification of surface stress and hence be important to general circulation (e.g.; Pierrehumbert and Wyman,1985, Baines and Palmer, 1990, Sandu et al. 2019). Lott and Miller (1997) described an orographic drag parameterization that incorporated the impact of near-surface nonlinearities due to flow diversion around obstacles (also referred to as blocking). The key elements in their approach are schematically illustrated in Figure 3. When mountain heights  $h_m$  exceed a critical value  $F_1 \left(\frac{U}{N}\right)$  a portion of the flow is assumed to be diverted or blocked. The depth of this layer is given by:

821

$$Z_B = \text{Max}(h_m - F_1 \frac{U}{N}, 0) \quad (12)$$

822  
823  
824  
825  
826  
827  
828

The parameter  $F_1$ , a critical non-dimensional mountain height or vertical displacement, is known from numerical and tank experiments to be of order 1 but may depend on obstacle shape. The forcing amplitude for vertically-propagating gravity waves in Lott and Miller (1997) is taken to be the full mountain height, however they suggest that this should be reduced to something approaching  $F_1(U/N)$  in three dimensional flows.



829  
830  
831  
832  
833  
834  
835  
836  
837  
838  
839  
840  
841  
842  
843  
844  
845  
846  
847  
848  
849  
850  
851  
852  
853  
854  
855  
856  
857  
858  
859  
860  
861  
862  
863  
864  
865  
866  
867  
868  
869  
870  
871  
872  
873

Within the blocked layer, Lott and Miller (1997) assume the drag follows a bluff-body law:

$$\frac{\partial U}{\partial t} \propto -\frac{1}{\bar{\rho}} \frac{\partial(\bar{\rho} \overline{u'w'})}{\partial z} = 0.5 \bar{\rho} C_d l(z) U |U| \quad (13)$$

Where  $C_d$  is a nondimensional drag coefficient close to 1 and  $l(z)$  is the cross-stream length presented by the obstacle. Lott and Miller (1997)'s formulation still employs a single wave.

The Scinocca and McFarlane (2000) parameterization employs two, instead of one, vertically propagating waves in order to provide a representation of the azimuthal distribution of momentum flux in the parameterized gravity-wave field launched by a ‘best-fit’ elliptical barrier, similarly to Lott and Miller (1997), but with a new way of defining unresolved topography. Scinocca and McFarlane (2000) also extended the representation of low-level drag to include enhancement by the downslope windstorm regimes. These flows are analogous to hydraulic supercritical flow (Smith 1989) and are thought to be related to near-surface wave breaking (e.g. Clark and Peltier 1977, Bacmeister and Pierrehumbert 1988). Three dimensional numerical studies cited by Scinocca and McFarlane (e.g.; Miranda and James 1992, Olafsson and Bougeault 1996) suggest that downslope winds with enhanced drag appear for a limited range of mountain heights, roughly for  $F_1 < Nh_m/U < 3F_1$ . In these flows the surface drag applied in the scheme is determined by

$$\tau_{sfc} = (1 + \beta(F))\tau_{lin} - \tau_c \quad (14)$$

where  $\tau_c$  is the moment flux carried by the freely propagating waves and  $\tau_{lin}$  is the nominal linear wave drag  $\sim \rho N U h_m^2 / L$ . This enhanced drag is applied via a linearly decreasing momentum flux profile in a layer from the surface to the first breaking level above the mountain. The height of this breaking level is approximated using linear theory. The enhancement factor  $\beta(F)$  peaks around  $F = Nh_m/U = 1.5F_1$  and has values between 2 and 4 depending on obstacle geometry. This parameterization of form drag can change the direction of the low-level flow to be more parallel to unresolved topographic ridges.

A new approach to orographic GW source parameterization is presented by van Niekerk et al. (2021), where they use the spectral, hydrostatic linear MW theory of Garner (2005) and Smith and Kruse (2018). Here, a two by two matrix of orographic GW drag coefficients are computed from the 2-D Fourier transform of the subgrid-scale terrain. Multiplication of the source-level wind vector with this drag matrix produces a source MW momentum flux vector that takes into account all subgrid scales and orographic anisotropy, eliminating the monochromatic assumption common to all previous MW drag parameterizations, at least at the source. Van Niekerk et al. (2021) further develop a parameterization for how the elements of the drag coefficient matrix depend on low-level blocking. Initial implementation in the Met Office Unified Model demonstrates this approach does a much better job at keeping total GW drag (resolved + parameterized) constant as grid resolution is changed relative to previous monochromatic parameterizations and improved weather prediction performance.



### 874 11.2.3.2 Convectively generated gravity waves

875

876 Source spectra parameterizations for convectively generated gravity waves were  
877 developed on the basis of the three dominant generation mechanisms: thermal forcing,  
878 mechanical oscillator, and obstacle effect (described in detail in Section 11.1.3). Rind et al.  
879 (1988) was first to implement a parameterization for nonstationary GWs linked to wave sources.  
880 The parameterization included waves generated by convection and wind shear based on  
881 theoretical assumptions. GW momentum flux of convectively generated GWs was related to the  
882 convective mass flux generated by the model. The phase speed of gravity waves was set to the  
883 mean wind over the convective region  $\pm 10 \text{ m s}^{-1}$ , and for deeper convection additional waves  
884 with phase speeds equal to the mean wind  $\pm 20 \text{ m s}^{-1}$  and  $\pm 40 \text{ m s}^{-1}$  were added. Kershaw  
885 (1995) developed a convective GW source parameterization which can be viewed as a  
886 parametrization of the obstacle effect as it focuses on parameterizing the effect of wave  
887 generation by flow over heating. A similar parameterization was developed by Chun and Baik  
888 (1998) parameterizing the effect of wave generation by mean flow over steady heating,  
889 representing only gravity waves that are stationary relative to the heat source. This  
890 parameterization was further extended to include effects of vertical wind shear by Chun and Baik  
891 (2002).

892 Beres et al. 2004 and Beres 2004 developed a parameterization of convectively generated  
893 GWs assuming that thermal forcing is the dominant GW generation mechanism. This method is  
894 based on linear theory and both steady and oscillatory components of the heating, are considered;  
895 hence stationary and non-stationary GWs, relative to the heating, are represented. The dominant  
896 spectral properties of the GWs depend on the horizontal and vertical scales of the heating. The  
897 dominant GW phase speed is primarily determined by the convective heating depth,  $h$ , leading  
898 to a dominant wave phase speed of  $\pm 15 \text{ m s}^{-1}$  for  $h = 5 \text{ km}$ , and a dominant wave phase speed  
899 of  $25 \text{ m s}^{-1}$  for  $h = 10 \text{ km}$  (assuming horizontal scale of heating of  $2.5 \text{ km}$ ). The horizontal scale  
900 of the heating primarily changes the amplitude and not the characteristics of the wave spectrum.  
901 The momentum flux of convectively generated GWs is proportional to the square of the heating.  
902 The effects of environmental wind in and above the convective region are also incorporated into  
903 the parameterization, as wind shear can create a large asymmetry in the GW spectrum (Beres et  
904 al. 2002). A similar parameterization was developed by Song and Chun (2005) based on a more  
905 complex vertical structure of the zonal mean wind and stability.

906 The convective source parameterizations by Beres et al. 2004 and Song and Chun (2005)  
907 based on thermal forcing are a large improvement over fixed source representations as they  
908 provide physically based connections between GWs and their evolving tropospheric sources, and  
909 hence, respond to changes in convection on all time scales including changes resulting from  
910 climate change. However, both of these parameterizations omit the effects of the nonlinear  
911 forcing (Chun et al. 2005). Chun et al. (2008) proposed a method of including the effects of  
912 nonlinear forcing effect on a spectrum of convectively generated GWs and showed that this  
913 inclusion reduced cloud top momentum flux by about 10%, except for middle latitude storm-  
914 tracks regions where the cloud-top momentum flux was amplified. Choi and Chun (2011)  
915 updated the Song and Chun (2005) parameterization by determining two free parameters of that  
916 parameterization: the moving speed of the convective source and the wave propagation direction.

917 Taking a slightly different approach, Lott and Guez (2013) developed a source spectrum  
918 parameterization for convectively generated GWs based on a stochastic approach presented in  
919 Eckermann (2011). In this approach, a few monochromatic waves chosen randomly from a

920 probability distribution are launched at each time step. The amplitudes of the waves are  
921 proportional to the square of the diabatic heating derived from the precipitation field. This  
922 approach leads to a wider range of wave amplitudes, leading to a lower level of momentum  
923 deposition as compared to uniform sources. In addition to the complex convective source  
924 parameterization described above, Bushell et al. (2015) implemented a relatively simple  
925 convective GW source representation by linking GW momentum flux amplitude to the square  
926 root of total precipitation. The introduction of the amplitude dependence generated launch-level  
927 flux amplitudes with greater spatial and temporal variability, increasing realism of parameterized  
928 convectively generated GWs.

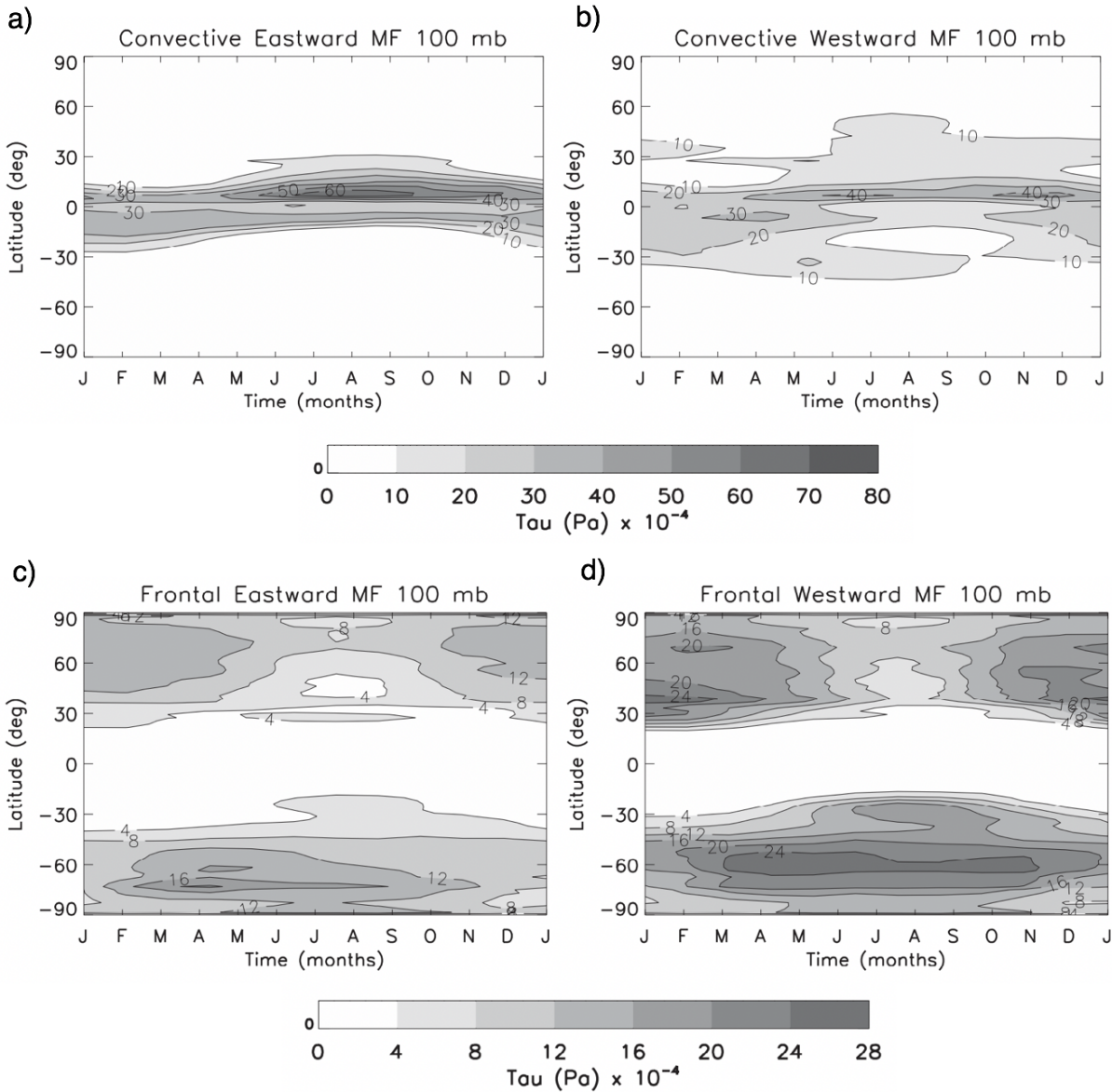
929 The inclusion of all of the above-described convective source parameterizations had a  
930 positive impact on simulations of climate in several GCMs. Parameterizations of Chun and Baik  
931 (1998) and Chun and Baik (2002) improved the representation of the middle atmosphere in the  
932 Yonsei University atmospheric GCM (YONU AGCM; Chun et al. 2001), the National Center for  
933 Atmospheric Research (NCAR) Community Climate Model (CCM) version 3 (Chun et al.  
934 2004)], and the National Centers for Environmental Prediction (NCEP) global spectral model  
935 (GSM) (Jeon et al (2010)). The Beres et al. (2005) was implemented in Whole Atmosphere  
936 Community Climate Model, version 2 (WACCM2) instead of the arbitrarily specified source  
937 spectra only in the tropics and resulted in an improved representation of the stratospheric semi-  
938 annual oscillation (SAO) (Beres et al. 2005). The Song and Chun (2005) parameterization was  
939 implemented in the Whole Atmosphere Community Climate Model, version 1b resulting in an  
940 alleviation of the model's zonal mean wind biases, primarily in the low to mid latitudes of the  
941 upper stratosphere and the mesosphere, and improving the structure and the magnitude of the  
942 SAO (Song et al. 2007). Choi and Chun (2013) demonstrated a reduction in wind biases and  
943 alleviation of cold temperature biases in the winter polar stratosphere using the Choi and Chun  
944 (2011) spectrum and the ray-based parameterization of Song and Chun (2008). Unfortunately,  
945 neither one of these parameterizations remedied the lack of an internally generated QBO in  
946 WACCM; However, a decade later, an internally generated QBO was generated with the Beres  
947 et al. (2005) parameterization in the Community Atmosphere Model, version 5 (Richter et al.  
948 2014), and subsequently in WACCM (Garcia and Richter 2019) but only after the vertical  
949 resolution of these models was doubled to  $\sim 500$  m in the free troposphere and lower  
950 stratosphere. The implementation of the Beres et al. (2004) parameterization in the ECHAM6  
951 model led to improvements of several aspects of the QBO. With the Lott and Guez (2013)  
952 parameterization, the LMDz model was able to obtain a QBO with vertical resolution in the  
953 stratosphere of  $\sim 500$  m. The modifications to the source level amplitudes by Bushell et al.  
954 (2015) led to the improved representation of the QBO in the UK Met Office global model.

955  
956  
957  
958  
959

### 960 **11.2.3.3 Gravity waves generated by jets/fronts**

961  
962 Parameterizations of GWs generated by jets/fronts are less developed and less common in GCMs  
963 as compared to parameterizations of orographic and convective gravity wave sources. As  
964 mentioned in the previous section, Rind et al. (1988) parameterized non-orographic GW sources  
965 by convection and shear. Shear-generated GWs were launched at jet stream level and assigned a

966 single wavenumber and phase speed in each GCM grid box dependent on the direction of the  
967 shear and wind velocity in the shear layers. Wave momentum flux magnitude was set to be  
968 proportional to the square of the wind shear between two successive layers. Subsequently,  
969 Charron and Manzini (2002) parameterized frontally generated gravity waves. They used the  
970 frontogenesis function (Miller 1948, Hoskins 1982) to diagnose the location of fronts. In this  
971 approach, GWs were launched at a fixed level of 600 hPa, and if the frontogenesis function  
972 exceeded a critical threshold, a relatively high gravity wave variance was imposed in two cross-  
973 front directions. At grid points where the frontogenesis function was not exceeded, GWs were  
974 launched with a much lower variance representing other possible GW sources. The  
975 implementation of this parameterization in the MAECHAM4 model produced a reasonable  
976 representation of the stratospheric and mesospheric dynamics. Richter et al. (2010) used a  
977 modified version of the Charron and Manzini (2002) approach to represent frontally generated  
978 GWs. They also used the frontogenesis function and a launching level of 600 hPa, and only  
979 launched frontally generated gravity waves when the frontogenesis threshold was exceeded, and  
980 no small amplitude spectrum was employed. In order to obtain enough drag in the  
981 stratosphere/mesosphere via this approach, the frontogenesis threshold used was ~ half of that  
982 used by Charron and Manzini (2002), however no additional background GW spectrum was  
983 used. Richter et al. (2010) used the Beres et al. (2004) convective GW parameterization as well,  
984 hence GWs in the Tropics were primarily generated from the convective scheme and in the  
985 extratropics from the frontal scheme. When the frontogenesis threshold was exceeded, a  
986 Gaussian GW momentum flux phase speed spectrum of constant value was launched. Hence the  
987 frontogenesis function was used to produce realistic spatial and temporal variability of frontally  
988 generated GWs, including seasonality. However, there was no relation between the properties of  
989 fronts and the properties of the GWs generated by them. Figure 4 shows the convective (top  
990 panels) and frontal (bottom panels) eastward and westward momentum flux at 100 hPa in the  
991 Whole Atmosphere Community Climate Model, version 3.5 (WACCM3.5) used in Richter et al.  
992 (2010). The figure clearly shows the dominance of convectively generated gravity waves in the  
993 tropics and of frontally generated gravity waves in the extratropics. Convectively generated GWs  
994 follow the seasonal cycle of tropical convection, with highest values of GW momentum flux in  
995 the NH winter (summer) primarily south (north) of the equator. Although the relationship  
996 between the spectrum of waves launched from fronts is not linked to their properties, the 100 hPa  
997 momentum flux reflects the seasonal cycle of frontal systems with a maximum in the winter  
998 season, and an asymmetry between eastward and westward propagating waves resulting from the  
999 strong filtering of eastward propagating GWs by strong tropospheric westerlies between 600 hPa  
1000 and 100 hPa.  
1001  
1002



1003  
 1004  
 1005

**Figure 4:** Total eastward (left panels) and westward (right panels) momentum flux (in Pa) for convectively (top panels) and frontally (bottom panels) generated gravity waves as a function of latitude and time of year derived from WACCM3.5. Figure adapted from Richter et al. (2010).

1009  
 1010  
 1011  
 1012  
 1013  
 1014  
 1015  
 1016  
 1017

Camara and Lott (2015) parameterized GW generation via spontaneous adjustment mechanism (described in section 11.1.4.) in combination with stochastic approach used in Lott and Guez (2013) to parameterize convective gravity wave sources. In this parameterization GW Eliassen-Palm flux is related to the amplitude and depth of potential vorticity anomalies, hence determining the location and amplitude of GWs. Even though spontaneous adjustment theory predicts exponentially small GW perturbations, the implementation of the scheme in LMDz provided enough extratropical wave drag to obtain reasonable circulations in the stratosphere and mesosphere (Camara and Lott 2015).

1018  
1019  
1020  
1021  
1022  
1023  
1024  
1025  
1026  
1027  
1028  
1029  
1030  
1031  
1032  
1033  
1034  
1035  
  
1036  
1037  
1038  
1039  
1040  
1041  
1042  
1043  
1044  
  
1045  
1046  
1047  
1048  
1049  
1050  
1051  
1052  
1053  
1054  
1055  
1056  
1057  
1058  
1059  
1060  
1061  
1062

#### 11.2.4 Uncertainties and parameter tuning

As GW drag parameterizations are designed, constants are inevitably involved in the derived relations. These constants are not always well constrained and, in practice, are often tuned (more below). Examples include horizontal wavenumber (estimated from unresolved orography in OGW parameterizations, a constant in non-orographic GW parameterizations) and a critical non-dimensional wave amplitude, defining a non-dimensional GW amplitude at which instabilities will begin dissipation. An additional “efficiency factor,”  $e$ , is typically introduced into GW parameterizations, having values between zero and unity. This term was introduced into early OGW parameterizations in order to reduce excessive MW drag in the lower stratosphere (e.g. Klinker and Sardeshmukh 1992). An efficiency factor is a common part of most GW parameterizations, both orographic and non-orographic. This factor is typically applied in one of two ways: 1)  $e$  is multiplied with the drag profile, reducing drag but not influencing the levels where the parameterized wave breaks or 2) just applied to the source-level momentum flux. The latter option reduces the wave amplitude, influencing initial breaking levels and where GW drag is exerted.

A variety of physical justifications for an efficiency factor have been put forward. GWs may occur intermittently within spatial and/or temporal grid scales. There can also be spectral intermittency, where the spectrum that is specified at the source may not be fully represented at all points and times. Mountains are 3-D and not 2-D, as treated by the parameterizations, which can reduce source-level momentum fluxes, as ridges are not necessarily perpendicular to the flow or the mountains represented could be more isolated. These real effects may result in reducing the momentum fluxes and drags below that predicted by the simple 2-D, steady, hydrostatic, instantaneous, Boussinesq, linear, monochromatic, only vertically-propagating, Wentzel-Kramer-Boussinesq theory upon which most GW parameterizations are based.

Ideally, the tuning constants involved should be constrained by observations. However, current observation platforms (aircraft, radiosondes, super-pressure balloons, satellite-borne nadir and limb sounders) have limited capability for quantitatively constraining 3-D GW characteristics and momentum flux globally due to low frequency in space and time and/or lack of sensitivity to the entire spectrum of GWs. Still, progress towards verifying GW parameterizations has been made in recent years with derivations of global GW momentum fluxes (e.g.: Vincent et al. 1997, Ern et al. 2004, Alexander et al. 2008, Hertzog et al 2008, Ern et al. 2017, Hindley et al. 2020). Geller et al. 2013 made a first attempt at comparing parameterized gravity wave momentum fluxes in climate models to gravity wave momentum fluxes derived from observations. This work focused on absolute momentum fluxes (sum over all directions) and showed a general good spatial agreement between models and global satellite estimates, but the observations were not yet able to provide meaningful constraints. Recent measurements from super-pressure balloon campaigns are able to derive GW momentum fluxes with higher accuracy (Jewtoukoff et al. 2013, 2015), but these are limited to a single level in the lower stratosphere, limited in latitude, and limited to campaign periods. Despite new sophisticated methods of analyzing satellite observations and estimating vector momentum fluxes, GW drag on the mean flow cannot be directly estimated from observations without orders of magnitude uncertainty (Alexander and Sato 2015).

1063  
1064 Without a direct way of measuring key quantities in GW drag parameterizations (i.e: momentum  
1065 flux as a function of wave direction and phase speed at the source level) globally, tuning  
1066 parameters are estimated indirectly. The free parameters are chosen to be physically reasonable  
1067 and then the mean wind and temperature of the middle atmosphere, which are relatively well  
1068 observed, provide an indirect verification measure for gravity wave parameterizations. In other  
1069 words, during the development of new versions of GCMs, gravity wave parameterizations are  
1070 ‘tuned’ in order to arrive at a reasonable representation of the observed zonal-mean climate.  
1071 Such an exercise assumes errors from other parts of the model (e.g. the dynamical core, other  
1072 parameterizations) are small, that the form of the GW drag parameterizations are correct, and  
1073 that errors that remain are attributable to the GW drag parameterizations and ultimately  
1074 incorrectly specified tuning parameters. These tuning parameters are adjusted in order to best  
1075 represent the observed mean climate. These assumptions are, of course, not valid; however, such  
1076 an exercise is common practice in developing climate models. Tuning of GW drag  
1077 parameterizations likely results in the GW parameterizations compensating for other model  
1078 errors (e.g. horizontal and vertical discretization errors, numerical diffusion, errors in other  
1079 parameterizations, errors in GW parameterization structure).

1080  
1081 Gravity wave tuning is an iterative process which consists of changing the unconstrained  
1082 parameterization parameters, running the climate model, and assessing model climatology and  
1083 biases. The process is repeated typically several to several dozen times until an acceptable  
1084 modeled climate state is achieved. Models with fixed GW sources typically have one set of  
1085 tunable parameters and with those they need to arrive at reasonable tropical and extratropical  
1086 mean wind and temperature in the stratosphere, and also in the mesosphere (if the model extends  
1087 this high). Despite many GW tuning efforts, many GCMs end up with a ‘cold-pole bias’ in the  
1088 Southern Hemisphere winter polar stratosphere (e.g: Eyring et al. (2006), Austin et al. (2003))  
1089 which can be improved by additional GW drag in the southern hemisphere (Garcia et al. 2017).  
1090 In addition, many recent climate models have internally generated QBOs which are largely  
1091 driven by parameterized gravity waves (e.g.: Giorgetta et al. 2006, Richter et al. 2014 and Geller  
1092 et al. 2016) and hence GW parameterization parameters must be just right to get a reasonable  
1093 period of the QBO close to observed in addition to the mean wind and temperature in the middle  
1094 atmosphere. Source oriented GW parameterizations allow more flexibility while tuning GWs, as  
1095 typically in models such as WACCM (Richter et al. 2010) and LMDz (Lott et al. 2012, Lott and  
1096 Guez 2013), convectively generated GWs control the Tropics: QBO and SAO, whereas the  
1097 orographic and frontal waves affect the extratropical mean state. More complexity and options  
1098 in GW parameterization parameters, however also means endless combinations of poorly  
1099 constrained parameters, which is also difficult to deal with.

1100

1101

### 1102 **11.2.5 Missing processes**

1103

1104 Again, GWs are treated as linear, hydrostatic, only propagating vertically (in a slowly-varying  
1105 background in z, no less), propagating upward instantaneously, and propagating through a steady  
1106 ambient environment with Boussinesq governing equations. All these simplifications lurking in  
1107 the underlying physics prevent representation of many GW characteristics that are well observed  
1108 and physically understood.



1109 For example, non-orographic GW observations show strong amplitude intermittency, where  
1110 infrequently observed waves with very large amplitudes can represent very high fractions of  
1111 time-averaged momentum flux. Indeed, from observations in the lower stratosphere (Hertzog et  
1112 al. 2012), distributions of individual event wave momentum fluxes have shown a log-normal  
1113 distribution of amplitudes, with the largest amplitude waves occurring <10% of the time but  
1114 carrying ~60% of the average flux. Such amplitude intermittency is generally not well  
1115 represented, or not represented at all, having important implications for the total momentum  
1116 fluxed and levels where it gets deposited. GW parameterizations that have GW sources tied to  
1117 particular mechanisms (e.g. convective parameterizations, frontogenesis metrics, MW  
1118 parameterizations, see following sections) do have some representation of intermittency, tied to  
1119 the intermittency of the sources represented by the host model. Still, the infrequent, but very  
1120 large-amplitude GWs remain underrepresented (e.g. Stephan et al. (2016)).

1121 Stochasticity in parameterized gravity wave sources is another way to account for wave  
1122 intermittency. Eckermann (2011) demonstrated that stochastic representation of the non-  
1123 orographic wave spectrum in different grid points gave similar middle atmospheric circulation  
1124 changes as including the full spectrum uniformly, but at much lower computational cost. These  
1125 ideas have found use in modern parameterization schemes (de la Camara et al. 2014, Serva et al.  
1126 2018) with some demonstrated improvements in model performance.

1127 Numerous other characteristics of GWs are unrepresented as a result of the many conventional,  
1128 and sometimes pragmatic, assumptions and simplifications made. Non-hydrostatic influences  
1129 occur when the GW intrinsic frequency becomes close to the buoyancy frequency and can reduce  
1130 orographic drag (e.g. Smith and Kruse 2017) and result in wave reflection and trapping, which  
1131 can also influence drag (see Section 8 of Tiexeira 2014 for an overview). Neglecting lateral-  
1132 propagation results in significant overestimates of MW amplitudes, breaking and drag at  
1133 altitudes that are too low, and drag that is too spatially confined (e.g. Eckermann et al. 2015b).  
1134 Trailing MWs launched terrain orientations oblique to the source-level flow can propagate  
1135 horizontally for O(1000) kilometers (e.g. Sato et al. 2012, Amemiya and Sato 2016, Jiang et al.  
1136 2019), and neglect of such long-distance propagation is likely in part responsible for an artificial  
1137 gap in GW drag near 60S in climate models that significantly influences Southern Hemisphere  
1138 polar night jet strength (McLandress et al. 2012, Kruse et al. 2021).

1139  
1140 Transience of both the GWs and their background can also be important. Transient forcing  
1141 results in vertical dispersion and spreading of GWs due to the spectrum of vertical group  
1142 velocities of the generated spectrum of GWs (e.g. Chen et al. 2007, Kruse and Smith 2018),  
1143 which influence wave amplitudes and breaking levels. Increasing and decreasing flow over  
1144 terrain result in MWs with positive and negative phase speeds and propagation downstream and  
1145 upstream of the mountains, respectively. Transient forcing also induces transient wave packet  
1146 propagation, allowing interaction of the GW packet with the environment it propagates into and  
1147 out of even without breaking (Fritts and Dunkerton 1984, Bühler and McIntyre 1999, 2003,  
1148 2005, Dosser and Sutherland 2011, Bölöni et al. 2016, Kruse and Smith 2018). Ray tracing  
1149 methods have been applied in research models to account for horizontal propagation and group  
1150 velocity effects (Song and Chun 2008, Bölöni et al. 2016), but these have not found wider  
1151 application because of computational costs.

1152

1153 To summarize, GWs are very important in Earth's atmosphere, and their representation in all  
1154 weather and climate models that do not fully resolve the entire GW spectrum is essential. The  
1155 various parameterizations implemented do improve weather and climate model skill. Still, there  
1156 is much potential to improve parameterizations via both better observational constraints and  
1157 improving the underlying physics.

1158

1159

### Acknowledgements

1160 CGK was supported by the National Science Foundation (NSF, grant #2004512) and in part by an  
1161 Advanced Study Program fellowship at the National Center for Atmospheric Research, which is  
1162 also supported by the NSF under Cooperative Agreement 1852977. JHR and JTB were supported  
1163 by NCAR as well. MJA was supported by both the NSF (grant #1829373) and NASA (grant  
1164 #80NSSC17K0169). The mountain wave simulation in Fig. 1 and Supplemental Animation 1 were  
1165 performed using high-performance computing support from Cheyenne ([doi:10.5065/D6RX99HX](https://doi.org/10.5065/D6RX99HX))  
1166 provided by NCAR's Computational and Information Systems Laboratory, sponsored by the  
1167 National Science Foundation. JW was supported by the National Natural Science Foundation of  
1168 China (Grant 42075005) and Guangdong Province Key Laboratory for Climate Change and  
1169 Natural Disaster Studies (Grant 2020B1212060025).

1170

1171

1172

### References

1173

1174 Alaka, M. A., 1960: *The Airflow Over Mountains*. WMO Technical Note No. 34. World  
1175 Meteorological Organization, Geneva. 137pp.

1176

1177 Adachi, Y., Yukimoto, S., Deushi, M., Obata, A., Nakano, H., Tanaka, T. Y., Hosaka, M.,  
1178 Sakami, T., Yoshimura, H., Hirabara, M., Shindo, E., Tsujino, H., Mizuta, R., Yabu, S., Koshiro,  
1179 T., Ose, T., and Kitoh, A.: Basic performance of a new earth system model of the Meteorological  
1180 Research Institute (MRI-ESM1), *Papers in Meteor. and Geophys.*, 64, 1–19, 2013.

1181

1182 Alexander, M. J., and T. J. Dunkerton, A spectral parameterization of mean-flow forcing due to  
1183 breaking gravity waves, *J. Atmos. Sci.*, 56, 4167–4182, 1999.

1184

1185 Alexander, M. J, J. R. Holton, and D. R. Durran, 1995: The gravity wave response above deep  
1186 convection in a squall line simulation. *J. Atmos. Sci.*, 52, 2212–2226.

1187

1188 Alexander M. J, and J. Holton, 1997: A model study of zonal forcing in the equatorial  
1189 stratosphere by convectively induced gravity waves. *J. Atmos. Sci.*, 54, 408–419.

1190

1191 Alexander M. J. and J. R. Holton, 2004: On the spectrum of vertically propagating gravity  
1192 waves generated by a transient heat source. *Atmospheric Chemistry and Physics Discussions*,  
1193 European Geosciences Union, 2004, 4 (1), pp.1063-1090.

1194

1195 Alexander, M. J., and D. A. Ortland (2010), Equatorial waves in High Resolution Dynamics  
1196 Limb Sounder (HIRDLS) data, *J. Geophys. Res.*, 115, D24111, doi:10.1029/2010JD014782.

1197



1198 Alexander, M., and K. Rosenlof, Nonstationary gravity wave forcing of the stratospheric zonal  
1199 mean wind, *J. Geophys. Res.*, 101, 23,465–23,474, 1996.  
1200

1201 Alexander, M. J., and K. H. Rosenlof (2003), Gravity wave forcing in the stratosphere:  
1202 Observational constraints from UARS and implications for parameterization in global models, *J.*  
1203 *Geophys. Res.*, 108(D19), doi:10.1029/2003JD003,373.  
1204

1205 Alexander, M. J., and Coauthors, 2008: Global estimates of gravity wave momentum flux from  
1206 High Resolution Dynamics Limb Sounder observations. *J. Geophys. Res.*, 113, D15S18,  
1207 doi:10.1029/2007JD008807.  
1208

1209 Alexander, M. J., and T. J. Dunkerton, 1999: A spectral parameterization of mean-flow forcing  
1210 due to breaking gravity waves, *J. Atmos. Sci.*, 56, 4167–4182  
1211

1212 Alexander, M. J., Eckermann, S. D., Broutman, D., and Ma, J. (2009), Momentum flux estimates  
1213 for South Georgia Island mountain waves in the stratosphere observed via satellite, *Geophys.*  
1214 *Res. Lett.*, 36, L12816, doi:[10.1029/2009GL038587](https://doi.org/10.1029/2009GL038587).  
1215

1216 Alexander, M. J. and K. Sato, [SPARC Newsletter No. 44](#), 2015, p. 9: Gravity Wave Dynamics  
1217 and Climate: An Update from the SPARC Gravity Wave Activity  
1218

1219 Amemiya, A and K. Sato, 2016: A new gravity wave parameterization including three-  
1220 dimensional propagation. *J. Meteorological Soc. of Japan*, Vol. 94, No. 3, pp. 237-256.  
1221 DOI:10.2151/jmsj.2016-013  
1222

1223 Austin, J., et al. (2003), Uncertainties and assessments of chemistry-climate models of the  
1224 stratosphere, *Atmos. Chem. Phys.*, 3, 1–27.  
1225

1226 Azeem, I., S. L. Vadas, G. Crowley, and J. J. Makela, 2017, Traveling ionospheric disturbances  
1227 over the United States induced by gravity waves from the 2011 Tohoku tsunami and comparison  
1228 with gravity wave dissipative theory, *J. Geophys. Res. Space Physics*, 122, 3430–3447,  
1229 doi:10.1002/2016JA023659.  
1230

1231 Bacmeister, J.T. and R.T. Pierrehumbert, 1988: On High-Drag States of Nonlinear Stratified  
1232 Flow over an Obstacle. *J. Atmos. Sci.*, **45**, 63–80, [https://doi.org/10.1175/1520-](https://doi.org/10.1175/1520-0469(1988)045<0063:OHDSON>2.0.CO;2)  
1233 [0469\(1988\)045<0063:OHDSON>2.0.CO;2](https://doi.org/10.1175/1520-0469(1988)045<0063:OHDSON>2.0.CO;2)  
1234

1235 Bacmeister, J. T., and M. R. Schoeberl, 1989: Breakdown of vertically propagating two-  
1236 dimensional gravity waves forced by orography. *J. Atmos. Sci.*, **46**, 2109–2134.  
1237

1238 Bacmeister, J. T., Mountain-wave drag in the stratosphere and mesosphere inferred from  
1239 observed winds and a simple mountain-wave parameterization scheme, *J. Atmos. Sci.*, 50, 377–  
1240 399, 1993.  
1241

1242 Baines, P. G., and T. N. Palmer, Rationale for a new physically-based parameterisation of sub-  
1243 grid scale orographic effects., Tech. Rep. 169, ECMWF (1990)

1244  
1245 Bakas, N., and B. Farrell (2008), Momentum and energy transport by gravity waves in  
1246 stochastically driven stratified flows. Part II: Radiation of gravity waves from a Gaussian jet, *J.*  
1247 *Atmos. Sci.*, *65*(7), 2308–2325.  
1248  
1249 Bakas, N., and B. Farrell (2009a), Gravity waves in a horizontal shear flow. Part I: Growth  
1250 mechanisms in the absence of potential vorticity perturbations., *J. Phys. Oceanogr.*, *39*, 481–496.  
1251  
1252 Bakas, N., and B. Farrell (2009b), Gravity waves in a horizontal shear flow. Part II: Interaction  
1253 between gravity waves and potential vorticity perturbations, *J. Phys. Oceanogr.*, *39*, 497–511.  
1254  
1255 Baldwin, M. P., et al. (2001), The quasi-biennial oscillation, *Rev. Geophys.*, *39*, 179–229.  
1256  
1257 Beljaars, A. C. M., Brown, A. R. and Wood, N. (2004), A new parametrization of turbulent  
1258 orographic form drag. *Q.J.R. Meteorol. Soc.*, *130*: 1327–1347. doi:10.1256/qj.03.73.  
1259  
1260 Beres, J. H., M. J. Alexander, and J. R. Holton, 2002: Effects of tropospheric wind shear on the  
1261 spectrum of convectively generated gravity waves. *J. Atmos. Sci.*, **59**, 1805–1824.  
1262  
1263 Beres, J. H., M. J. Alexander, and J. R. Holton, 2004: A method of specifying the gravity wave  
1264 spectrum above convection based on latent heating properties and background wind. *J. Atmos.*  
1265 *Sci.*, **61**, 324–337.  
1266  
1267 Beres J. H., 2004: Gravity Wave Generation by a Three-Dimensional Thermal Forcing. *Journal*  
1268 *of the Atmospheric Sciences* **61**:14, 1805-1815.  
1269  
1270 Beres, J. H., R. R. Garcia, B. A. Boville, and F. Sassi (2005), Implementation of a gravity wave  
1271 source spectrum parameterization dependent on the properties of convection in the Whole  
1272 Atmosphere Community Climate Model (WACCM), *J. Geophys. Res.*, *110*, D10108,  
1273 doi:10.1029/2004JD005504.  
1274  
1275 Boer, G. J., N. A. McFarlane, R. Laprise, J. D. Henderson and J.-P. Blanchet. 1984. The  
1276 Canadian Climate Centre spectral atmospheric general circulation model. *Atmosphere-Ocean*,  
1277 **22**: 397–429.  
1278  
1279 Bossert K., C. Kruse, C. Heale, D. C. Fritts, J. Snively P.-D. Pautet, B. P. Williams, M. J. Taylor  
1280 (2017), Secondary Gravity Wave Generation Over New Zealand During the DEEPWAVE  
1281 Campaign, *J. Geophys. Res. Atmos.*, doi:10.1002/2016JD026079.  
1282  
1283 Bossert, K., Fritts, D. C., Heale, C. J., Eckermann, S. D., Plane, J. M. C., Snively, J. B., et al.  
1284 (2018). Momentum flux spectra of a mountain wave event over New Zealand. *Journal of*  
1285 *Geophysical Research: Atmospheres*, *123*, 9980–9991. [https://doi-](https://doi-org.cuucar.idm.oclc.org/10.1029/2018JD028319)  
1286 [org.cuucar.idm.oclc.org/10.1029/2018JD028319](https://doi-org.cuucar.idm.oclc.org/10.1029/2018JD028319)  
1287

1288 Bőlöni, G., B. Ribstein, J. Muraschko, C. Sgoff, J. Wei, and U. Achatz, 2016: The interaction  
1289 between atmospheric gravity waves and large-scale flows: An efficient description beyond the  
1290 nonacceleration paradigm. *J. Atmos. Sci.*, 73, 4833–4852, doi:10.1175/JAS-D-16-0069.1.  
1291

1292 Boville, B. 1986. Wave-mean flow interactions in a general circulation model of the troposphere  
1293 and stratosphere. *J. Atmos. Sci.* **43**: 1711–1725.  
1294

1295 Boville, B. A. (1991), Sensitivity of simulated climate to model resolution, *J. Climate*, 4,  
1296 469–485.  
1297

1298 Bretherton, C.: Group velocity and the linear response of stratified fluids to internal heat or mass  
1299 sources, *J. Atmos. Sci.*, 45, 81–93, 1988.  
1300

1301 Bretherton, C. S., and P. K. Smolarkiewicz, 1989: Gravity waves, compensating subsidence and  
1302 detrainment around cumulus clouds. *J. Atmos. Sci.*, **46**, 740–759.

1303 Bramberger, M., Dörnbrack, A., Bossert, K., Ehard, B., Kaifler, B., Mallaun, C., ... Witschas, B.  
1304 (2017). Does Strong tropospheric forcing cause large-amplitude mesospheric gravity waves? A  
1305 DEEPWAVE case study. *Journal of Geophysical Research: Atmospheres*, 122, 11,422–11,443.  
1306 <https://doi.org/10.1002/2017JD027371>  
1307

1308 Broutman, D., S. D. Eckermann, H. Knight, and J. Ma (2017), A stationary phase solution for  
1309 mountain waves with application to mesospheric mountain waves generated by Auckland Island,  
1310 *J. Geophys. Res. Atmos.*, 122, 699–711, doi:[10.1002/2016JD025699](https://doi.org/10.1002/2016JD025699).  
1311

1312 Bühler, O., and M. E. McIntyre, 1999: On shear-generated gravity waves that reach the  
1313 mesosphere. part II: Wave propagation. *J. Atmos. Sci.*, 56, 3764–3773.  
1314

1315 Bühler, O., and M. E. McIntyre, 2003: Remote recoil: a new wave-mean interaction effect. *J.*  
1316 *Fluid Mech.*, 492, 207–230.  
1317

1318 Bühler, O., and M. E. McIntyre, 2005: Wave capture and wave-vortex duality. *J. Fluid Mech.*,  
1319 534, 67–95, doi:10.1017/S0022112005004374.  
1320

1321 Bühler, O., M. McIntyre, and J. Scinocca (1999), On shear-generated gravity waves that reach  
1322 the mesosphere. Part I: Wave generation, *J. Atmos. Sci.*, 56, 3749–3763.  
1323

1324 Burleigh, M. R., Heale, C. J., Zettergren, M. D., & Snively, J. B. (2018). Modulation of low-  
1325 altitude ionospheric upflow by linear and nonlinear atmospheric gravity waves. *Journal of*  
1326 *Geophysical Research: Space Physics*, 123. <https://doi.org/10.1029/2018JA025721>  
1327

1328 Bushell, A. C., Butchart, N., Derbyshire, S. H., Jackson, D. R., Shutts, G. J., Vosper, S. B., &  
1329 Webster, S. (2015). Parameterized gravity wave momentum fluxes from sources related to  
1330 convection and large-scale precipitation processes in a global atmosphere model. *Journal of the*  
1331 *Atmospheric Sciences*, 72(11), 4349–4371.  
1332

1333 Bushell, AC, Anstey, JA, Butchart, N, et al. Evaluation of the Quasi-Biennial Oscillation in  
1334 global climate models for the SPARC QBO-initiative. *QJR Meteorol*  
1335 *Soc.* 2020; 1– 31. <https://doi.org/10.1002/qj.3765>  
1336

1337 Butchart, N., and J. Austin, Middle atmosphere climatologies from the troposphere-stratosphere  
1338 configuration of the ukmo’s unified model, *J. Atmos. Sci.*, 55, 2782–2809, 1998.  
1339

1340 Butchart, N., Anstey, J., Hamilton, K., Osprey, S., McLandress, C., Bushell, A., Kawatani, Y.,  
1341 Kim, Y.-H., Lott, F., Scinocca, J., Stockdale, T., Andrews, M., Bellprat, O., Braesicke, P.,  
1342 Cagnazzo, C., Chen, C.-C., Chun, H.-Y., Dobrynin, M., Garcia, R., Garcia-Serrano, J., Gray, L.,  
1343 Holt, L., Kerzenmacher, T., Naoe, H., Pohlmann, H., Richter, J., Scaife, A., Schenzinger, V.,  
1344 Serva, F., Versick, S., Watanabe, S., Yoshida, K. and Yukimoto, S. (2018) Overview of  
1345 experiment design and comparison of models participating in phase 1 of the SPARC Quasi-  
1346 Biennial Oscillation initiative (QBOi). *Geoscientific Model Development*, 11, 1009–1032.  
1347

1348 de la Cámara A., F. Lott and A. Hertzog, Intermittency in a stochastic parameterization of  
1349 nonorographic gravity waves, *Journal of Geophysical Research: Atmospheres*, 119, 21, (11,905-  
1350 11,919), (2014).  
1351

1352 Cámara, A. and F. Lott, A parameterization of gravity waves emitted by fronts and  
1353 jets, *Geophysical Research Letters*, 42, 6, (2071-2078), (2015).  
1354

1355 Cámara, A. d. l., Lott, F., Jewtoukoff, V., Plougonven, R., & Hertzog, A. (2016). On the Gravity  
1356 Wave Forcing during the Southern Stratospheric Final Warming in LMDZ, *Journal of the*  
1357 *Atmospheric Sciences*, 73(8), 3213-3226.  
1358

1359 Charron, M. and E. Manzini, 2002: Gravity Waves from Fronts: Parameterization and Middle  
1360 Atmosphere Response in a General Circulation Model. *J. Atmos. Sci.*, 59,923–941,  
1361 [https://doi.org/10.1175/1520-0469\(2002\)059<0923:GWFFPA>2.0.CO;2](https://doi.org/10.1175/1520-0469(2002)059<0923:GWFFPA>2.0.CO;2)  
1362

1363 Chen, C.-C., D. R. Durran, and G. J. Hakim, 2005: Mountain-wave momentum flux in an  
1364 evolving synoptic-scale flow. *J. Atmos. Sci.*, 62, 3213–3231, <https://doi.org/10.1175/JAS3543.1>.  
1365 Chen, C., Hakim, G. J., & Durran, D. R. (2007). Transient Mountain Waves and Their  
1366 Interaction with Large Scales, *Journal of the Atmospheric Sciences*, 64(7), 2378-2400.  
1367

1368 Chimonas, G., and J. Grant (1984), Shear excitation of gravity waves. Part II: Upscale scattering  
1369 from Kelvin-Helmholtz waves, *J. Atmos. Sci.*, 41, 2278–2288.  
1370

1371 H. -J. Choi and H. -Y. Chun. (2013) Effects of Convective Gravity Wave Drag in the Southern  
1372 Hemisphere Winter Stratosphere. *Journal of the Atmospheric Sciences* 70:7, 2120-2136.  
1373

1374 Chun, H.-Y., and J.-J. Baik, 1998: Momentum flux by thermally induced internal gravity waves  
1375 and its approximation for large-scale models. *J. Atmos. Sci.*, 55, 3299–3310.  
1376

1377 Chun, H-Y., M-D. Song, J-W. Kim, and J-J. Baik, 2001a: Effects of gravity wave drag induced  
1378 by cumulus convection on the atmospheric general circulation. *J. Atmos. Sci.*, 58, 302–319.

1379  
1380 Chun, H.-Y., and J.-J. Baik, 2002: An updated parameterization of convectively forced gravity  
1381 wave drag for use in large-scale models. *J. Atmos. Sci.*, **59**, 1006–1017.  
1382  
1383 Chun, H.-Y., I.-S. Song, J.-J Baik, and Y.-J. Kim, (2004) Impact of a Convectively Forced  
1384 Gravity Wave Drag Parameterization in NCAR CCM3. *Journal of Climate* **17**:18, 3530-3547.  
1385  
1386 Chun, H.-Y., J.-J. Baik, and T. Horinouchi, 2005: Momentum flux spectrum of convectively  
1387 forced gravity waves: Can diabatic forcing be a proxy for convective forcing? *J. Atmos. Sci.*, **62**,  
1388 4113–4120  
1389  
1390 Chun, H.-Y., and Y.-H. Kim(2008), Secondary waves generated by breaking of convective  
1391 gravity waves in the mesosphere and their influence in the wave momentum flux, *J. Geophys.*  
1392 *Res.*, **113**, D23107, doi:[10.1029/2008JD009792](https://doi.org/10.1029/2008JD009792)  
1393  
1394 Chun, H.-Y., H.-J. Choi, and I.-S. Song, 2008: Effects of nonlinearity on convectively forced  
1395 internal gravity waves: Application to a gravity wave drag parameterization. *J. Atmos. Sci.*, **65**,  
1396 557–575, doi:<https://doi.org/10.1175/2007JAS2255.1>.  
1397  
1398 Choi H.-J. and H.-Y. Chun. (2011) Momentum Flux Spectrum of Convective Gravity Waves.  
1399 Part I: An Update of a Parameterization Using Mesoscale Simulations. *Journal of the*  
1400 *Atmospheric Sciences* **68**:4, 739-759.  
1401  
1402 Clark, T.L. and W.R. Peltier, 1977: On the Evolution and Stability of Finite-Amplitude  
1403 Mountain Waves. *J. Atmos. Sci.*, **34**, 1715–1730, [https://doi.org/10.1175/1520-](https://doi.org/10.1175/1520-0469(1977)034<1715:OTEASO>2.0.CO;2)  
1404 [0469\(1977\)034<1715:OTEASO>2.0.CO;2](https://doi.org/10.1175/1520-0469(1977)034<1715:OTEASO>2.0.CO;2)  
1405  
1406 Clark, T.L. and W.R. Peltier, 1984: Critical Level Reflection and the Resonant Growth of  
1407 Nonlinear Mountain Waves. *J. Atmos. Sci.*, **41**, 3122–3134, [https://doi.org/10.1175/1520-](https://doi.org/10.1175/1520-0469(1984)041<3122:CLRATR>2.0.CO;2)  
1408 [0469\(1984\)041<3122:CLRATR>2.0.CO;2](https://doi.org/10.1175/1520-0469(1984)041<3122:CLRATR>2.0.CO;2)  
1409  
1410 Clark, T. L., T. Hauf, and J. P. Kuettnner, 1986: Convectively forced internal gravity waves:  
1411 Results from two-dimensional numerical experiments. *Quart. J. Roy. Meteor. Soc.*, **112**, 899–925  
1412  
1413 Choi H.-J. and H.-Y. Chun. (2011) Momentum Flux Spectrum of Convective Gravity Waves.  
1414 Part I: An Update of a Parameterization Using Mesoscale Simulations. *Journal of the*  
1415 *Atmospheric Sciences* **68**:4, 739-759.  
1416  
1417 Davini, P., von Hardenberg, J., Corti, S., Christiansen, H. M., Juricke, S., Subramanian, A.,  
1418 Watson, P. A. G., Weisheimer, A., and Palmer T. N.: Climate SPHINX: evaluating the impact of  
1419 resolution and stochastic physics parameterisations in the EC-EARTH global climate model,  
1420 *Geosci. Model Dev.* **10**, 1383–1402, doi:10.5194/gmd-10-1383-2017, 2017.  
1421  
1422 Dörnbrack, A., M. Leutbecher, R. Kivi, and E. Kyrö, Mountain- wave induced record low  
1423 stratospheric temperatures above northern Scandinavia, *Tellus, Ser. A*, **51**, 951–963, 1999.  
1424

1425 Dossier, H. V., and B. R. Sutherland, 2011: Anelastic internal wave packet evolution and  
1426 stability. *J. Atmos. Sci.*, 68, 2844–2859, doi:10.1175/JAS-D-11-097.1.  
1427

1428 Drazin P. G. (1961) On the steady flow of a fluid of variable density past an obstacle. *Tellus*  
1429 13:239–251  
1430

1431 Dunkerton, T. J. (1982), Theory of the mesopause semiannual oscillation, *J. Atmos. Sci.*, 39,  
1432 2681–2690.  
1433

1434 Dunkerton, T. J. (1997), The role of gravity waves in the quasi-biennial oscillation, *J. Geophys.*  
1435 *Res.*, 102(D22), 26,053–26,076.  
1436

1437 Durran, D.R. and J.B. Klemp, 1983: A Compressible Model for the Simulation of Moist  
1438 Mountain Waves. *Mon. Wea. Rev.*, **111**, 2341–2361, [https://doi.org/10.1175/1520-](https://doi.org/10.1175/1520-0493(1983)111<2341:ACMFTS>2.0.CO;2)  
1439 [0493\(1983\)111<2341:ACMFTS>2.0.CO;2](https://doi.org/10.1175/1520-0493(1983)111<2341:ACMFTS>2.0.CO;2)  
1440

1441 Durran, D.R., 1986: Mountain Waves (Mesoscale Meteorology and Forecasting). American  
1442 Meteorological Society, Boston, pp 472-492.  
1443

1444 Durran, D.R., 1986a: Another look at downslope windstorms. Part I: On the development of  
1445 analogs to supercritical flow in an infinitely deep continuously stratified fluid. *J. Atmos. Sci.*, 93,  
1446 2527-2543.  
1447

1448 Durran, D.R., 1986b: Mountain Waves (Mesoscale Meteorology and Forecasting). American  
1449 Meteorological Society, Boston, pp 472-492.  
1450

1451 Durran, D.R. and J.B. Klemp, 1987: Another Look at Downslope Winds. Part II: Nonlinear  
1452 Amplification beneath Wave-Overturning Layers. *J. Atmos. Sci.*, **44**, 3402–  
1453 3412, [https://doi.org/10.1175/1520-0469\(1987\)044<3402:ALADWP>2.0.CO;2](https://doi.org/10.1175/1520-0469(1987)044<3402:ALADWP>2.0.CO;2)  
1454

1455 Durran, D.R. 1990. Mountain waves and downslope winds. In: *Atmospheric Processes over*  
1456 *Complex Terrain*. W. Blumen, (Ed), Meteorol. Monogr. Am. Meteorol. Soc. 23 (45): 59–81.  
1457

1458 Durran, D. R. 2003. Lee waves and mountain waves. *Encyclopedia of Atmospheric Sciences*  
1459 (eds. J. R. Holton, J. Pyle and J. A. Curry). Elsevier Science Ltd., London, 1161-1170.  
1460

1461 Eckermann, S. D. (2011), Explicitly stochastic parameterization of nonorographic gravity wave  
1462 drag, *J. Atmos. Sci.*, 68, 1749–1765.  
1463

1464 Eckermann, S. D., J. Ma, and D. Broutman, 2015: Effects of horizontal geometrical spreading on  
1465 the parameterization of orographic gravity wave drag. Part I: Numerical transform solutions. *J.*  
1466 *Atmos. Sci.*, 72, 2330–2347, <https://doi.org/10.1175/JAS-D-14-0147.1>.  
1467

1468 Eckermann, S. D., Broutman, D., & Knight, H. (2015). Effects of Horizontal Geometrical  
1469 Spreading on the Parameterization of Orographic Gravity Wave Drag. Part II: Analytical



1470 Solutions, *Journal of the Atmospheric Sciences*, 72(6), 2348-2365. Retrieved Oct 7, 2021,  
1471 from <https://journals.ametsoc.org/view/journals/atsc/72/6/jas-d-14-0148.1.xml>  
1472

1473 Eckermann, S.D., D. Broutman, J. Ma, J.D. Doyle, P. Pautet, M.J. Taylor, K. Bossert, B.P.  
1474 Williams, D.C. Fritts, and R.B. Smith, 2016: Dynamics of Orographic Gravity Waves Observed  
1475 in the Mesosphere over the Auckland Islands during the Deep Propagating Gravity Wave  
1476 Experiment (DEEPWAVE). *J. Atmos. Sci.*, **73**, 3855–3876, [https://doi.org/10.1175/JAS-D-16-](https://doi.org/10.1175/JAS-D-16-0059.1)  
1477 0059.1  
1478

1479 Eliassen, A., and E. Palm, 1960: On the transfer of energy in stationary mountain waves. *Geofys.*  
1480 *Publ.*, 22 (3), 1–23.  
1481

1482 Ern, M., P. Preusse, M. J. Alexander, and C. D. Warner, 2004: Absolute values of gravity wave  
1483 momentum flux derived from satellite data. *J. Geophys. Res.*, 109, D20103,  
1484 doi:10.1029/2004JD004752.

1485 Ern, M., L. Hoffmann, and P. Preusse, 2017: Directional gravity wave momentum fluxes in the  
1486 stratosphere derived from high-resolution AIRS temperature data. *Geophys. Res. Lett.*, **44** (1),  
1487 475–485, <https://doi.org/10.1002/2016GL072007>.

1488 Eyring, V., and Coauthors, 2006: Assessment of temperature, trace species, and ozone in  
1489 chemistry-climate model simulations of the recent past. *J. Geophys. Res.*, **111**, D22308.  
1490 doi:10.1029/2006JD007327.  
1491

1492 Eyring, V., et al. (2007), Multimodel projections of stratospheric ozone in the 21st Century, *J.*  
1493 *Geophys. Res.*, 112(D16303), doi:10.1029/2006JD008,332.  
1494

1495 Farmer, D. M. & Armi, L. (1999): The generation and trapping of solitary waves over  
1496 topography. *Science* **283**, 188–190  
1497

1498 Felten, F. N., and T. S. Lund (2006), Kinetic energy conservation issues associated with the  
1499 collocated mesh scheme for incompressible flow, *J. Comput. Phys.*, 215, 465–484.  
1500

1501 Ford, R., M. E. McIntyre, and W. A. Norton (2000), Balance and the slow quasi manifold: Some  
1502 explicit results, *J. Atmos. Sci.*, 57, 1236–1254.  
1503

1504 Ford, R., 1994a: Gravity wave radiation from vortex trains in rotating shallow water, *J. Fluid*  
1505 *Mech.*, 281, 81–118.  
1506

1507 Ford, R., 1994b: The response of a rotating ellipse of uniform potential vorticity to gravity wave  
1508 radiation, *Phys. Fluids*, 6(11), 3694–3704.  
1509

1510

1511 Fovell, R., D. Durran, and J. R. Holton, 1992: Numerical simulations of convectively generated  
1512 stratospheric gravity waves. *J. Atmos. Sci.*, **49**, 1427–1442  
1513

1514 Fovell, R. G., Mullendore, G. L., & Kim, S. (2006). Discrete Propagation in Numerically  
1515 Simulated Nocturnal Squall Lines, *Monthly Weather Review*, 134(12), 3735-3752.  
1516

1517 Franke, P. M., and W. A. Robinson(1999),Nonlinear behavior in the propagation of atmospheric  
1518 gravity waves, *J. Atmos. Sci.*,56, 3010–3027.  
1519

1520 Fritts, D. C., and Z. Luo (1992), Gravity wave excitation by geostrophic adjustment of the jet  
1521 stream. Part I: Two-dimensional forcing, *J. Atmos. Sci.*, 49(8), 681–697.  
1522

1523 Fritts, D. C., & Dunkerton, T. J. (1984). A Quasi-Linear Study of Gravity-Wave Saturation and  
1524 Self-Acceleration, *Journal of Atmospheric Sciences*, 41(22), 3272-3289.  
1525

1526 Fritts, D. (1984), Shear excitation of atmospheric gravity waves. 2: Nonlinear radiation from a  
1527 free shear layer, *J. Atmos. Sci.*, 41, 524–537.  
1528

1529 Fritts, D. C., and W. Lu, Spectral estimates of gravity wave energy and momentum fluxes, II,  
1530 Parameterization of wave forcing and variability, *J. Atmos. Sci.*, 50, 3695–3713, 1993.  
1531

1532 Fritts, D. C., and Alexander, M. J. (2003), Gravity wave dynamics and effects in the middle  
1533 atmosphere, *Rev. Geophys.*, 41, 1003, doi:[10.1029/2001RG000106](https://doi.org/10.1029/2001RG000106), 1.  
1534

1535 Fritts, D.C., R.B. Smith, M.J. Taylor, J.D. Doyle, S.D. Eckermann, A. Dörnbrack, M. Rapp, B.P.  
1536 Williams, P. Pautet, K. Bossert, N.R. Criddle, C.A. Reynolds, P.A. Reinecke, M. Uddstrom, M.J.  
1537 Revell, R. Turner, B. Kaifler, J.S. Wagner, T. Mixa, C.G. Kruse, A.D. Nugent, C.D. Watson, S.  
1538 Gisinger, S.M. Smith, R.S. Lieberman, B. Laughman, J.J. Moore, W.O. Brown, J.A. Haggerty,  
1539 A. Rockwell, G.J. Stosmeister, S.F. Williams, G. Hernandez, D.J. Murphy, A.R. Klekociuk,  
1540 I.M. Reid, and J. Ma, 2016: The Deep Propagating Gravity Wave Experiment (DEEPWAVE):  
1541 An Airborne and Ground-Based Exploration of Gravity Wave Propagation and Effects from  
1542 Their Sources throughout the Lower and Middle Atmosphere. *Bull. Amer. Meteor. Soc.*, 97, 425–  
1543 453, <https://doi.org/10.1175/BAMS-D-14-00269.1>  
1544

1545 Fritts, D. C., Vosper, S. B., Williams, B. P., Bossert, K., Plane, J. M. C., Taylor, M. J., et al.  
1546 (2018). Large-amplitude mountain waves in the mesosphere accompanying weak cross-mountain  
1547 flow during DEEPWAVE Research Flight RF22. *Journal of Geophysical Research:*  
1548 *Atmospheres*, 123, 9992–10,022. <https://doi.org/10.1029/2017JD028250>  
1549

1550 Garcia, R.R. and J.H. Richter, 2019: On the Momentum Budget of the Quasi-Biennial  
1551 Oscillation in the Whole Atmosphere Community Climate Model. *J. Atmos. Sci.*, 76,69–87,  
1552 <https://doi.org/10.1175/JAS-D-18-0088.1>  
1553

1554 Garcia, R. R., and B. A. Boville (1994), “Downward control” of the mean meridional  
1555 circulation and temperature distribution of the polar winter stratosphere, *J. Atmos. Sci.*, 51,  
1556 2238–2245.  
1557



1558 Garcia, R. R., and S. Solomon, The effect of breaking gravity waves on the dynamics and  
1559 chemical composition of the mesosphere and lower thermosphere, *J. Geophys. Res.*, *90*, 3850–  
1560 3868, 1985.

1561

1562 Garcia R. G. , A. K. Smith, D. E. Kinnison, Á. de la Cámara, and D. J. Murphy, 2017:  
1563 Modification of the gravity wave parameterization in the Whole Atmosphere Community  
1564 Climate Model: Motivation and results. *J. Atmos. Sci.*, *74*, 275–291, doi:[10.1175/JAS-D-16-0104.1](https://doi.org/10.1175/JAS-D-16-0104.1).

1565

1566

1567 Garfinkel, C. I., & Oman, L. D. ( 2018). Effect of gravity waves from small islands in the  
1568 Southern Ocean on the Southern Hemisphere atmospheric circulation. *Journal of Geophysical*  
1569 *Research: Atmospheres*, *123*, 1552–1561,  
1570 <https://doi.org/10.1002/2017JD027576>.

1571 Garner, S. T., 2005: A topographic drag closure built on an ana- lytical base flux. *J. Atmos. Sci.*,  
1572 *62*, 2302–2315, [https://doi.org/ 10.1175/JAS3496.1](https://doi.org/10.1175/JAS3496.1).

1573 Geller, M.A., M.J. Alexander, P.T. Love, J. Bacmeister, M. Ern, A. Hertzog, E. Manzini, P.  
1574 Preusse, K. Sato, A.A. Scaife, and T. Zhou, 2013: A Comparison between Gravity Wave  
1575 Momentum Fluxes in Observations and Climate Models. *J. Climate*, *26*, 6383–6405,  
1576 <https://doi.org/10.1175/JCLI-D-12-00545.1>

1577

1578 Geller, M.A., T.H. Zhou, D. Shindell, R. Ruedy, I. Aleinov, L. Nazarenko, N. Tausnev, M.  
1579 Kelley, S. Sun, Y. Cheng, R.D. Field, and G. Faluvegi, 2016: Modeling the QBO —  
1580 Improvements resulting from higher model vertical resolution. *J. Adv. Model. Earth Syst.*, *8*, no.  
1581 *3*, 1092–1105, doi:10.1002/2016MS000699.

1582

1583 Gettelman, A., Mills, M. J., Kinnison, D. E., Garcia, R. R., Smith, A. K., Marsh, D. R., et al.  
1584 (2019). The whole atmosphere community climate model version 6 (WACCM6). *Journal of*  
1585 *Geophysical Research:*  
1586 *Atmospheres*, *124*, 12380– 12403. <https://doi.org/10.1029/2019JD030943>

1587

1588 Giorgetta, M. A., L. Bengtsson, and K. Arpe (1999), An investigation of QBO signals in the east  
1589 Asian and Indian monsoon in GCM experiments, *Clim. Dyn.*, *15*(6), 435–450,  
1590 doi:10.1007/s003820050292.

1591

1592 Giorgetta, M. A., E. Manzini, E. Roeckner, M. Esch, and L. Bengtsson (2006), Climatology and  
1593 forcing of the quasi-biennial oscillation in the MACHAM5 model, *J. Clim.*, *19*, 3882–3901.

1594

1595 Gossard, E.E., and William H. Hooke, 1975: Waves in the Atmosphere. Elsevier, New York,  
1596 456pp.

1597

1598 Guest, F.M., M.J. Reeder, C.J. Marks, and D.J. Karoly. 2000. Inertia-gravity waves observed in  
1599 the lower stratosphere over Macquarie Island. *J. Atmos. Sci.* *57*: 737–752.

1600 Heale, C. J., Snively, J. B., Hickey, M. P., & Ali, C. J. (2014). Thermospheric dissipation of  
1601 upward propagating gravity wave packets. *Journal of Geophysical Research: Space Physics*,  
1602 *119*, 3,857–3,872. <https://doi.org/10.1002/2013JA019387>

1603 Heale, C. J., and J. B. Snively (2015), Gravity wave propagation through a vertically and  
1604 horizontally inhomogeneous background wind, *J. Geophys. Res. Atmos.*, *120*, 5931–5950,  
1605 doi:10.1002/2015JD023505.

1606 Heale, C. J., K. Bossert, J. B. Snively, D. C. Fritts, P.-D. Pautet, and M. J. Taylor (2017),  
1607 Numerical modeling of a multiscale gravity wave event and its airglow signatures over Mount  
1608 Cook, New Zealand, during the DEEPWAVE campaign, *J. Geophys. Res. Atmos.*, *122*, 846–860,  
1609 doi: 10.1002/2016JD025700.

1610  
1611 Heale, C. J., Walterscheid, R. L., & Snively, J. B. (2018). Localization effects on the  
1612 dissipation of gravity wave packets in the upper mesosphere and lower thermosphere. *Journal of*  
1613 *Geophysical Research: Atmospheres*, *123*, 8915–8935. <https://doi.org/10.1029/2017JD027617>  
1614

1615 Heale, C. J., Lund, T., & Fritts, D. C. (2020). Convectively generated gravity waves during  
1616 solstice and equinox conditions. *Journal of Geophysical Research: Atmospheres*, *125*,  
1617 e2019JD031582. <https://doi.org/10.1029/2019JD031582>  
1618

1619 Hertzog, A., G. Boccara, R. A. Vincent, F. Vial, and P. Cocquerez, 2008: Estimation of gravity-  
1620 wave momentum fluxes and phase speeds from quasi-Lagrangian stratospheric balloon flights. 2:  
1621 Results from the Vorcore campaign in Antarctica. *J. Atmos. Sci.*, *65*, 3056–3070.  
1622

1623 Hindley, N. P., C. J. Wright, L. Hoffmann, T. Moffat-Griffin, and N. J. Mitchell, 2020: An 18-  
1624 year climatology of directional stratospheric gravity wave momentum flux from 3-d satellite  
1625 obser- vations. *Geophys. Res. Lett.*, **47** (22),  
1626 <https://doi.org/https://doi.org/10.1029/2020GL089557>.

1627 Hitchman, M. H., and C. B. Leovy (1988), Estimation of the Kelvin wave contribution to the  
1628 semiannual oscillation, *J. Atmos. Sci.*, *45*, 1462 – 1475.  
1629

1630 Hickey, M. P., R. L. Walterscheid, and G. Schubert (2011), Gravity wave heating and cooling of  
1631 the thermosphere: Sensible heat flux and viscous flux of kinetic energy, *J. Geophys. Res.*, *116*,  
1632 A12326, doi: <https://doi.org/10.1029/2011JA016792>  
1633

1634 Hines, C. O. (1997a). Doppler-spread parameterization of gravity-wave momentum deposition in  
1635 the middle atmosphere. Part 1: Basic formulation. *Journal of Atmospheric and Solar-Terrestrial*  
1636 *Physics*, *59*(4), 371–386. [https://doi.org/10.1016/S1364-6826\(96\)00079-X](https://doi.org/10.1016/S1364-6826(96)00079-X)  
1637

1638 Hines, C. O. (1997b). Doppler-spread parameterization of gravity-wave momentum deposition in  
1639 the middle atmosphere. Part 2: Broad and quasi monochromatic spectra, and implementation.  
1640 *Journal of Atmospheric and Solar-Terrestrial Physics*, *59*(4), 387–400.  
1641

1642 Hoffmann, L., Xue, X., and Alexander, M. J. (2013), A global view of stratospheric gravity wave  
1643 hotspots located with Atmospheric Infrared Sounder observations, *J. Geophys. Res.*  
1644 *Atmos.*, 118, 416– 434, doi:[10.1029/2012JD018658](https://doi.org/10.1029/2012JD018658).  
1645

1646 Hoffmann, L., Grimsdell, A. W., and Alexander, M. J.: Stratospheric gravity waves at Southern  
1647 Hemisphere orographic hotspots: 2003–2014 AIRS/Aqua observations, *Atmos. Chem. Phys.*, 16,  
1648 9381–9397, <https://doi.org/10.5194/acp-16-9381-2016>, 2016.  
1649

1650 Holt, L. A., M. J. Alexander, M. J., L. Coy, C. Liu, A. Molod, W. Putman, and S. Pawson, 2017:  
1651 An evaluation of gravity waves and their sources in the Southern Hemisphere in a 7-km global  
1652 climate simulation, *Q. J. Meteorol. Soc.*, 143(707), 2481–2495, doi:10.1002/qj.3101.  
1653

1654 Holton, J. R., 1982, The role of gravity wave induced drag and diffusion in the momentum  
1655 budget of the mesosphere, *J. Atmos. Sci.*, 39, 791–799.  
1656

1657 Holton, J. R., The influence of gravity wave breaking on the general circulation of the middle  
1658 atmosphere, *J. Atmos. Sci.*, 40, 2497–2507, 1983.  
1659

1660 Holton, J. R., and M. J. Alexander, 1999: Gravity waves in the mesosphere generated by  
1661 tropospheric convection. *Tellus*, 51A-B, 45–58.  
1662

1663 Holton, J. R., J. H. Beres, and X. Zhou, 2002: On the vertical scale of gravity waves excited by  
1664 localized thermal forcing. *J. Atmos. Sci.*, 59, 2019–2023, doi:[https://doi.org/10.1175/1520-0469\(2002\)059<2019:OTVSOG>2.0.CO;2](https://doi.org/10.1175/1520-0469(2002)059<2019:OTVSOG>2.0.CO;2).  
1665

1666 Holton, J. R., 2004: An Introduction to Dynamic Meteorology. 4<sup>th</sup> Edition. Volume 88 of  
1667 International Geophysics Series. Elsevier Inc.  
1668

1669 Hoskins, B. J., 1982: The mathematical theory of frontogenesis. *Annu. Rev. Fluid Mech.*, 14,  
1670 131–151.  
1671

1672 Hughes, M., A. Hall, and J. Kim, 2009: Anthropogenic reductions of Santa Ana winds.  
1673 California Climate Change Center Rep. CEC-500-2009-015-D, 19 pp.,  
1674 [www.energy.ca.gov/2009publications/CEC-500-2009-015/CEC-500-2009-015-D.pdf](http://www.energy.ca.gov/2009publications/CEC-500-2009-015/CEC-500-2009-015-D.pdf).  
1675

1676 Huppert, H., & Miles, J. (1969). Lee waves in a stratified flow Part 3. Semi-elliptical  
1677 obstacle. *Journal of Fluid Mechanics*, 35(3), 481-496. doi:10.1017/S0022112069001236  
1678

1679 Jiang, Q., J. D. Doyle, S. D. Eckermann, and B. P. Williams, 2019: Stratospheric trailing gravity  
1680 waves from New Zealand. *J. Atmos. Sci.*, in press.  
1681

1682 Jewtoukoff, V., Plougonven, R., and Hertzog, A. ( 2013), Gravity waves generated by deep  
1683 tropical convection: Estimates from balloon observations and mesoscale simulations, *J. Geophys.*  
1684 *Res. Atmos.*, 118, 9690– 9707, doi:10.1002/jgrd.50781.  
1685

1686

1687 Jewtoukoff, V., A. Hertzog, R. Plougonven, A.d. Cámara, and F. Lott, 2015: Comparison of  
1688 Gravity Waves in the Southern Hemisphere Derived from Balloon Observations and the  
1689 ECMWF Analyses. *J. Atmos. Sci.*, **72**, 3449–3468, <https://doi.org/10.1175/JAS-D-14-0324.1>  
1690

1691 Jeon J., S-Y Hong, H-Y Chun, and I-S Song. (2010) Test of a convectively forced gravity wave  
1692 drag parameterization in a general circulation model. *Asia-Pacific Journal of Atmospheric*  
1693 *Sciences* **46**:1, 1-10.  
1694

1695 Jiang Q., J. D. Doyle, S. Eckermann and B. P. Williams., 2019:  
1696 Stratospheric Trailing Gravity Waves from New Zealand. *JAS*, under review.  
1697

1698 Jin, Y. (1997), A numerical model study of the role of mesoscale gravity waves in rainband  
1699 dynamics in the central United States during STORM-FEST, PhD dissertation, North Carolina  
1700 State University.  
1701

1702 Kaifler, B., N. Kaifler, B. Ehard, A. Dörnbrack, M. Rapp, and D. C. Fritts (2015), Influences of  
1703 source conditions on mountain wave penetration into the stratosphere and mesosphere, *Geophys.*  
1704 *Res. Lett.*, **42**, 9488–9494, doi:[10.1002/2015GL066465](https://doi.org/10.1002/2015GL066465).  
1705

1706 Kaplan, M., S. Koch, Y.-L. Lin, R. Weglarz, and R. Rozumalski (1997), Numerical Simulations  
1707 of a Gravity Wave Event over CCOPE. Part I: The role of geostrophic adjustment in Mesoscale  
1708 Jetlet Formation, *Mon. Weather Rev.*, **125**, 1185–1211.  
1709

1710 Kawatani, Y., Watanabe, S., Sato, K., Dunkerton, T. J., Miyahara, S. and Takahashi, M. (2010)  
1711 The Roles of Equatorial Trapped Waves and Internal Inertia–Gravity Waves in Driving the  
1712 Quasi-Biennial Oscillation. Part II: Three-Dimensional Distribution of Wave Forcing. *Journal of*  
1713 *the Atmospheric Sciences*, **67**, 981–997.  
1714

1715 Kershaw, R., Parameterization of momentum transport by convectively generated gravity waves,  
1716 *Q. J. R. Meteorol. Soc.*, **121**, 1023–1040, 1995.  
1717

1718 Kim, Y. -J. and J. D. Doyle, 2005: Extension of an orographic-drag parameterization scheme to  
1719 incorporate orographic anisotropy and flow blocking. *Quart. J. Roy. Meteor. Soc.*, **131**, 1893–  
1720 1921, <https://doi.org/10.1256/qj.04.160>.  
1721

1722 Klinker, E., & Sardeshmukh, P. D. (1992). The Diagnosis of Mechanical Dissipation in the  
1723 Atmosphere from Large-Scale Balance Requirements, *Journal of Atmospheric Sciences*, **49**(7),  
1724 608-627. Retrieved Oct 8, 2021, from [https://journals.ametsoc.org/view/journals/atsc/49/7/1520-  
1725 0469\\_1992\\_049\\_0608\\_tdomdi\\_2\\_0\\_co\\_2.xml](https://journals.ametsoc.org/view/journals/atsc/49/7/1520-0469_1992_049_0608_tdomdi_2_0_co_2.xml)  
1726

1727 2016 Kruse, C. G., R. B. Smith, and S. D. Eckermann: The Mid-Latitude Lower-Stratospheric  
1728 Mountain Wave “Valve Layer”. *Journal of the Atmospheric Sciences*, **73**, 5081-5100.  
1729 doi:10.1175/JAS-D-16-0173.1.  
1730

1731 Kruse, C.G. and R.B. Smith, 2018: Nondissipative and Dissipative Momentum Deposition by  
1732 Mountain Wave Events in Sheared Environments. *J. Atmos. Sci.*, **75**, 2721–2740,  
1733 <https://doi.org/10.1175/JAS-D-17-0350.1>  
1734

1735 Kruse. C. G., M. J. Alexander, L. Hoffmann, A. van Niekerk, I. Polichtchouk, J. T. Bacmeister,  
1736 L. Holt, R. Plougonven, P. Sacha, C. Wright, K. Sato, R. Shibuya, S. Gisinger, M. Ern, C. I.  
1737 Meyer, and O. Stein, 2021: Observed and modeled mountain waves from the surface to the  
1738 mesosphere near the Drake Passage. *J. Atmos. Sci.*, Under review. JAS-D-21-0252.  
1739

1740 Lac, C., J. P. Lafore, and J. L. Redelsperger, 2002: Role of gravity waves in triggering deep  
1741 convection during TOGA COARE. *J. Atmos. Sci.*, **59**, 1293–1316,  
1742 doi:[https://doi.org/10.1175/1520-0469\(2002\)059<1293:ROGWIT>2.0.CO;2](https://doi.org/10.1175/1520-0469(2002)059<1293:ROGWIT>2.0.CO;2).  
1743

1744 Lane, T. P., and M. J. Reeder, 2001: Convectively generated gravity waves and their effect on  
1745 the cloud environment. *J. Atmos. Sci.*, **58**, 2427–2440.  
1746

1747 Lane, T. P., M. J. Reeder, and T. L. Clark, 2001: Numerical modeling of gravity wave generation  
1748 by deep tropical convection. *J. Atmos. Sci.*, **58**, 1249–1274, doi:[https://doi.org/10.1175/1520-0469\(2001\)058<1249:NMOGWG>2.0.CO;2](https://doi.org/10.1175/1520-0469(2001)058<1249:NMOGWG>2.0.CO;2).  
1749

1750

1751 Lane, T. P., and R. D. Sharman(2006), Gravity wave breaking, secondary wave generation, and  
1752 mixing above deep convection in a three-dimensional cloud model, *Geophys. Res. Lett.*, **33**,  
1753 L23813, doi:[10.1029/2006GL027988](https://doi.org/10.1029/2006GL027988).  
1754

1755 Lane T. P. , and F. Zhang, 2011: Coupling between gravity waves and tropical convection at  
1756 mesoscales. *J. Atmos. Sci.*, **68**, 2582– 2598, doi:[10.1175/2011JAS3577.1](https://doi.org/10.1175/2011JAS3577.1).  
1757

1758 Leo, L. S., Thompson, M. Y., Di Sabatino, S. & Fernando, H. J. S. 2016 Stratified flow past a  
1759 hill: dividing streamline concept revisited. *Boundary-Layer Meteorol.* **159** (3), 611–634.  
1760

1761 Lelong, M. and T.J. Dunkerton, 1998: Inertia–Gravity Wave Breaking in Three Dimensions. Part  
1762 II: Convectively Unstable Waves. *J. Atmos. Sci.*, **55**, 2489–2501, [https://doi.org/10.1175/1520-0469\(1998\)055<2489:IGWBIT>2.0.CO;2](https://doi.org/10.1175/1520-0469(1998)055<2489:IGWBIT>2.0.CO;2)  
1763

1764

1765 Leutbecher, M., and H. Volkert, Propagation of mountain waves into the stratosphere:  
1766 Quantitative evaluation of three-dimensional simulations, *J. Atmos. Sci.*, **57**, 3090–  
1767 3108, 2000.  
1768

1769 Lighthill, J. M., 1952: On sound generated aerodynamically, I. General theory, *Proc. Roy. Soc.*  
1770 London, **211**(A), 564–587.  
1771

1772 Lilly, D.K., 1978: A Severe Downslope Windstorm and Aircraft Turbulence Event Induced by a  
1773 Mountain Wave. *J. Atmos. Sci.*, **35**, 59–77, [https://doi.org/10.1175/1520-0469\(1978\)035<0059:ASDWAA>2.0.CO;2](https://doi.org/10.1175/1520-0469(1978)035<0059:ASDWAA>2.0.CO;2)  
1774

1775

1776 Lilly, D., & Klemp, J. (1979). The effects of terrain shape on nonlinear hydrostatic mountain  
1777 waves. *Journal of Fluid Mechanics*, 95(2), 241-261. doi:10.1017/S0022112079001452  
1778  
1779 Lilly, D. K., and P. J. Kennedy, Observations of a stationary mountain wave and its associated  
1780 momentum flux and energy dissipation, *J. Atmos. Sci.*, 30, 1135–1152, 1973  
1781  
  
  
  
  
  
1782 Lin, Y.-L., R. L. Deal, and M. S. Kulie, 1998: Mechanisms of cell regeneration, development,  
1783 and propagation within a two-dimensional multicell storm. *J. Atmos. Sci.*, **55**, 1867–1886.  
1784  
1785  
1786 Lin, Y.-L., and T. A. Wang, 1996: Flow regimes and transient dynamics of two-dimensional  
1787 stratified flow over an isolated mountain ridge. *J. Atmos. Sci.*, **53**, 139–158.  
1788  
1789 Lindzen, R. S., Turbulence and stress owing to gravity wave and tidal breakdown, *J. Geophys.*  
1790 *Res.*, 86, 9707–9714, 1981.  
1791  
1792 Liu, H.-L. and S. L. Vadas, 2013: "Large-scale ionospheric disturbances due to the dissipation of  
1793 convectively-generated gravity waves over Brazil", *J. Geophys. Res.*, 118, 2419–2427,  
1794 doi:10.1002/jgra.50244.  
1795  
1796 Lott, F. (1997), The transient emission of propagating gravity waves by a stably stratified shear  
1797 layer, *Q. J. R. Meteorol. Soc.*, 123,  
1798 1603–1619  
1799  
1800 Lott, F. (1998): Linear mountain drag and averaged pseudo-momentum flux profiles in the  
1801 presence of trapped lee waves. *Tellus*, 50A, 12–25.  
1802  
1803 Lott, F. and Miller, M (1997): A new sub-grid orographic drag parametrization: Its formulation  
1804 and testing. *Q. J. R. Meteorol. Soc.*, 123, 101-127  
1805  
1806 Lott, F., R. Plougonven, and J. Vanneste (2010), Gravity waves generated by sheared potential  
1807 vorticity anomalies, *J. Atmos. Sci.*, 67, 157–170, doi:10.1175/2009JAS3134.1.  
1808  
1809 Lott, F., R. Plougonven, and J. Vanneste (2012), Gravity waves generated by sheared three-  
1810 dimensional potential vorticity anomalies, *J. Atmos. Sci.*, 69, 2134–2151.  
1811  
1812 Lott, F., Guez, L., and Maury, P.: A stochastic parameterization of non-orographic gravity  
1813 waves, Formalism and impact on the equatorial stratosphere, *Geophys. Res. Lett.*, 39, L06807,  
1814 doi:10.1029/2012GL051001, 2012.  
1815  
1816 Lott F. and L. Guez. (2013) A stochastic parameterization of the gravity waves due to convection  
1817 and its impact on the equatorial stratosphere. *Journal of Geophysical Research: Atmospheres*  
1818 **118**:16, 8897-8909.

Luo, Z., and D. Fritts (1993), Gravity wave excitation by geostrophic adjustment of the jet  
stream. Part II: Three dimensional forcing, *J. Atmos. Sci.*, 50(1), 104–115.



1819  
1820 Lyra, G. 1940 Über den Einfluß von Bodenerhebungen auf die Strömung einer stabil  
1821 geschichteten Atmosphäre. *Beitr. Phys. Freien Atmos.* 26, 197–206.  
1822  
1823 Lyra, G., 1943: Theorie der stationären Leewellen- strömung in freier Atmosphäre, *Zeit. angew.*  
1824 *Math. Mech.*, 23, 1–28.  
1825  
1826 McFarlane, N.A. 1987. The effect of orographically excited gravity-wave drag on the general  
1827 circulation of the lower stratosphere and troposphere. *J. Atmos. Sci.* 44: 1775–1800.  
1828  
1829 McLandress, C., On the importance of gravity waves in the middle atmosphere and their  
1830 parameterization in general circulation models, *J. Atmos. Sol. Terr. Phys.*, 60, 1357–1383, 1998.  
1831  
1832 Medvedev, A. S., and G. P. Klaassen, Vertical evolution of gravity wave spectra and the  
1833 parameterization of associated wave drag, *J. Geophys. Res.*, 100, 25,841–25,853, 1995.  
1834  
1835 Medvedev AS, Yiğit E. Gravity Waves in Planetary Atmospheres: Their Effects and  
1836 Parameterization in Global Circulation Models. *Atmosphere*. 2019; 10(9):531.  
1837 <https://doi.org/10.3390/atmos10090531>  
1838  
1839 Miller, J. E., 1948: On the concept of frontogenesis. *J. Meteor.*, 5, 169 –171.  
1840  
1841 Miranda, P. M. A. and James, I. N. 1992. Non-linear three-dimensional effects on gravity wave  
1842 drag: splitting flow and breaking waves. *Quart. J. Roy. Meteorol. Soc.* 118, 1057-1081  
1843  
1844 Miyoshi, Y., H. Fujiwara, H. Jin, and H. Shinagawa (2014), A global view of gravity waves in  
1845 the thermosphere simulated by a general circulation model, *J. Geophys. Res. Space Physics*, 119,  
1846 5807–5820, doi: 10.1002/2014JA019848.  
1847  
1848 McFarlane, N. A., 1987: The effect of orographically excited wave drag on the general  
1849 circulation of the lower stratosphere and troposphere. *J. Atmos. Sci.*, 44, 1775–1800.  
1850  
1851 McLandress, C., T.G. Shepherd, S. Polavarapu, and S.R. Beagley, 2012: Is Missing Orographic  
1852 Gravity Wave Drag near 60°S the Cause of the Stratospheric Zonal Wind Biases in Chemistry–  
1853 Climate Models?. *J. Atmos. Sci.*, 69, 802–818, <https://doi.org/10.1175/JAS-D-11-0159.1>  
1854  
1855 Mixa, T., Dörnbrack, A., & Rapp, M. (2021). Nonlinear Simulations of Gravity Wave Tunneling  
1856 and Breaking over Auckland Island, *Journal of the Atmospheric Sciences*, 78(5), 1567-1582.  
1857 Retrieved Sep 30, 2021, from <https://journals.ametsoc.org/view/journals/atms/78/5/JAS-D-20-0230.1.xml>  
1858  
1859  
1860 Okamoto, K., K. Sato, and H. Akiyoshi (2011), A study on the formation and trend of the  
1861 Brewer-Dobson circulation, *J. Geophys. Res.*, 116, D10117, doi:10.1029/2010JD014953.  
1862  
1863 Ólafsson, H. and P. Bougeault, 1996: Nonlinear flow past an elliptic mountain ridge, *J. Atmos.*  
1864 *Sci.*, 53, 2465-2489



1865  
1866 Palmer, T. N., G. J. Shutts, and R. Swinbank, Alleviation of a systematic westerly bias in general  
1867 circulation and numerical weather prediction models through an orographic gravity wave drag  
1868 parameterization, *Q. J. R. Meteorol. Soc.*, 112, 1001–1039, 1986.  
1869  
1870 Pandya, R. E., and D. R. Durran, 1996: The influence of convectively generated thermal forcing  
1871 on the mesoscale circulation around squall lines. *J. Atmos. Sci.*, 53, 2924–2951,  
1872 doi:[10.1175/1520-0469\(1996\)053,2924:TIOCGT.2.0.CO;2](https://doi.org/10.1175/1520-0469(1996)053,2924:TIOCGT.2.0.CO;2).  
1873  
1874 Pandya, R. and Alexander, M.J. 1999.: Linear stratospheric gravity waves above convective  
1875 thermal Forcing, *J. Atmos. Sci.*, 56, 2434–2446, 1999.  
1876  
1877 Pautet, P.-D., M. J. Taylor, D. C. Fritts, K. Bossert, B. P. Williams, D. Broutman, J. Ma, S. D.  
1878 Eckermann, and J. D. Doyle (2016), Large-amplitude mesospheric response to an orographic  
1879 wave generated over the Southern Ocean Auckland Islands (50.7°S) during the DEEPWAVE  
1880 project, *J. Geophys. Res. Atmos.*, 121, 1431–1441, doi:10.1002/2015JD024336.  
1881  
1882 Peltier, W.R. and T.L. Clark, 1979: The Evolution and Stability of Finite-Amplitude Mountain  
1883 Waves. Part II: Surface Wave Drag and Severe Downslope Windstorms. *J. Atmos. Sci.*, 36,  
1884 1498–1529, [https://doi.org/10.1175/1520-0469\(1979\)036<1498:TEASOF>2.0.CO;2](https://doi.org/10.1175/1520-0469(1979)036<1498:TEASOF>2.0.CO;2)  
1885  
1886 Pfister, L.; S. Scott and M. Loewenstein. 1993. Mesoscale disturbances in the tropical  
1887 stratosphere excited by convection: Observations and effects on the stratospheric momentum  
1888 budget. *J. Atmos. Sci.* **50**: 1058–1075.  
1889  
1890 Phillips, D. S., 1984: Analytical surface pressure and drag for linear hydrostatic flow over three-  
1891 dimensional elliptical mountains. *J. Atmos. Sci.*, 41, 1073–1084, [https://doi.org/ 10.1175/1520-](https://doi.org/10.1175/1520-0469(1984)041,1073:ASPADF.2.0.CO;2)  
1892 [0469\(1984\)041,1073:ASPADF.2.0.CO;2](https://doi.org/10.1175/1520-0469(1984)041,1073:ASPADF.2.0.CO;2).  
1893  
1894 Piani, C., D. Durran, M. Alexander, and J. Holton, 2000: A numerical study of three-dimensional  
1895 gravity waves triggered by deep tropical convection and their role in the dynamics of the QBO. *J.*  
1896 *Atmos. Sci.*, 57, 3689–3702, doi:[10.1175/1520-0469\(2000\)057,3689: ANSOTD.2.0.CO;2](https://doi.org/10.1175/1520-0469(2000)057,3689:ANSOTD.2.0.CO;2).  
1897  
1898 Piani, C., and D. Durran, 2001: A numerical study of stratospheric gravity waves triggered by  
1899 squall lines observed during the TOGA COARE and COPT-81 experiments. *J. Atmos. Sci.*, 58,  
1900 3702–3723.  
1901  
1902 Pierrehumbert, R. T., and B. Wyman, 1985: Upstream effects of mesoscale mountains. *J. Atmos.*  
1903 *Sci.*, 42, 977–1003.  
1904  
1905 Plougonven, R., A. Hertzog, and M. J. Alexander, 2015: Case studies of nonorographic gravity  
1906 waves over the Southern Ocean emphasize the role of moisture. *J. Geophys. Res. Atmos.*, 120,  
1907 1278–1299, doi:10.1002/2014JD022332.  
1908

1909 Plougonven, R., Zeitlin, V., 2002: Internal gravity wave emission from a pancake vortex: an  
1910 example of wave-vortex interaction in strongly stratified flows. *Phys. of Fluids* 14(3), 1259–  
1911 1268.

1912

1913 Portele, T.C., A. Dörnbrack, J.S. Wagner, S. Gisinger, B. Ehard, P. Pautet, and M. Rapp, 2018:  
1914 Mountain-Wave Propagation under Transient Tropospheric Forcing: A DEEPWAVE Case  
1915 Study. *Mon. Wea. Rev.*, **146**, 1861–1888, <https://doi.org/10.1175/MWR-D-17-0080.1>

1916

1917 Powers, J., and R. Reed (1993), Numerical simulation of the large-amplitude mesoscale gravity  
1918 wave event of 15 December 1987 in the Central United States, *Mon. Weather Rev.*, *121*, 2285–  
1919 2308.

1920

1921 Plougonven, R., H. Teitelbaum, and V. Zeitlin (2003), Inertia-gravity wave generation by the  
1922 tropospheric mid-latitude jet as given by the  
1923 FASTEX radiosoundings, *J. Geophys. Res.*, *108*(D21), 4686, doi:10.1029/2003JD003535.

1924

1925 Plougonven, R., and F. Zhang, 2014: Internal gravity waves from atmospheric jets and fronts.  
1926 *Rev. Geophys.*, *52*, doi:[10.1002/2012RG000419](https://doi.org/10.1002/2012RG000419).

1927

1928 Powers, J. (1997), Numerical model simulation of a mesoscale gravity-wave event: Sensitivity  
1929 tests and spectral analyses, *Mon. Weather Rev.*, *125*, 1838–1869.

1930

1931 Queney, P. (1947), Theory of perturbations in stratified currents with applications to airflow over  
1932 mountain barriers. Dept. of Meteorology. Univ. of Chicago, Misc. Report No. 23

1933

1934 Ray, E. A., M. J. Alexander, and J. R. Holton (1998), An analysis of structure and forcing of the  
1935 equatorial semiannual oscillation in zonal wind, *J. Geophys. Res.*, *103*(D2), 1759–1774.

1936

1937 Richter, J., and R. R. Garcia (2006), On the forcing of the mesospheric semi-annual oscillation in  
1938 the Whole Atmosphere Community Climate Model, *Geophys. Res. Lett.*, *33*, L01806,  
1939 doi:[10.1029/2005GL024378](https://doi.org/10.1029/2005GL024378).

1940

1941 Richter, J. H., Sassi, F. and Garcia, R. R. (2010) Towards a physically based gravity wave source  
1942 parameterization in a general  
1943 circulation model. *J. Atmos. Sci.*, **67**, 136–156.

1944

1945 Richter, J. H., A. Solomon, and J. T. Bacmeister (2014), On the simulation of the quasi-biennial  
1946 oscillation in the Community Atmosphere Model, version 5, *J. Geophys. Res. Atmos.*, *119*,  
1947 3045–3062, doi:10.1002/2013JD021122.

1948

1949 Rind, D., R. Suozzo, N. K. Balachandran, A. Lacis, and G. Russell, 1988: The GISS global  
1950 climate-middle atmosphere model. Part I: Model structure and climatology. *J. Atmos. Sci.*, **45**,  
1951 329–370.

1952

1953 Rosenlof, K. (1996), Summer hemisphere differences in temperature and transport in the lower  
1954 stratosphere, *J. Geophys. Res.*, *101*, 19,129–19,136.

1955

1956 Ruppert, J. H., Jr., Koch, S. E., Chen, X., Du, Y., Seimon, A., Sun, Y. Q., Wei, J., and Bosart, L.

1957 F., 2021: Mesoscale Gravity Waves and Midlatitude Weather: A tribute to Fuqing Zhang,

1958 Bulletin of the American Meteorological Society (published online ahead of print 2021).

1959 from [https://journals.ametsoc.org/view/journals/bams/aop/BAMS-D-20-0005.1/BAMS-D-](https://journals.ametsoc.org/view/journals/bams/aop/BAMS-D-20-0005.1/BAMS-D-20-0005.1.xml)

1960 [20-0005.1.xml](https://journals.ametsoc.org/view/journals/bams/aop/BAMS-D-20-0005.1/BAMS-D-20-0005.1.xml)

1961

1962 Sandu, I., van Niekerk, A., Shepherd, T.G. *et al.* Impacts of orography on large-scale

1963 atmospheric circulation. *npj Clim Atmos Sci* **2**, 10 (2019). [https://doi.org/10.1038/s41612-019-](https://doi.org/10.1038/s41612-019-0065-9)

1964 [0065-9](https://doi.org/10.1038/s41612-019-0065-9)

1965

1966 Sato, K. (1994), A statistical study of the structure, saturation and sources of inertio-gravity

1967 waves in the lower stratosphere observed with the MU radar, *J. Atmos. Terr. Phys.*, *56*(6), 755–

1968 774.

1969

1970 Sato, K., Tateno, S., Watanabe, S., & Kawatani, Y. (2012). Gravity Wave Characteristics in the

1971 Southern Hemisphere Revealed by a High-Resolution Middle-Atmosphere General Circulation

1972 Model, *Journal of the Atmospheric Sciences*, *69*(4), 1378-1396. Retrieved Sep 30, 2021,

1973 from <https://journals.ametsoc.org/view/journals/atsc/69/4/jas-d-11-0101.1.xml>

1974

1975 Satomura, T. and K. Sato, 1999: [Secondary Generation of Gravity Waves Associated with the](https://doi.org/10.1175/1520-0469(1999)056<3847:SGOGWA>2.0.CO;2)

1976 [Breaking of Mountain Waves](https://doi.org/10.1175/1520-0469(1999)056<3847:SGOGWA>2.0.CO;2). *J. Atmos. Sci.*, *56*, 3847–3858, [https://doi.org/10.1175/1520-](https://doi.org/10.1175/1520-0469(1999)056<3847:SGOGWA>2.0.CO;2)

1977 [0469\(1999\)056<3847:SGOGWA>2.0.CO;2](https://doi.org/10.1175/1520-0469(1999)056<3847:SGOGWA>2.0.CO;2)

1978 Schirber, S., E. Manzini, and M. J. Alexander (2014), A convection-based gravity wave

1979 parameterization in a general circulation model: Implementation and improvements on the QBO,

1980 *J. Adv. Model. Earth Syst.*, *6*, 264–279, doi:10.1002/2013MS000286.

1981 Schmidt, J., and W. Cotton (1990), Interactions between upper and lower tropospheric gravity

1982 waves on squall line structure and maintenance, *J. Atmos. Sci.*, *47*, 1205–1222.

1983 Scinocca, J., and R. Ford (2000), The nonlinear forcing of large-scale internal gravity waves by

1984 stratified shear instability, *J. Atmos. Sci.*, *57*, 653–672.

1985

1986 Shige, S. and T. Satomura (2000), The Gravity Wave Response in the Troposphere around Deep

1987 Convection, *J. Met. Japan*, *78*(6), 789-801. [https://doi.org/10.2151/jmsj1965.78.6\\_789](https://doi.org/10.2151/jmsj1965.78.6_789)

1988

1989 Schecter, D., 2008: The spontaneous imbalance of an atmospheric vortex at high Rossby

1990 number. *J. Atmos. Sci.* *65*, 2498– 2521.

1991

1992 J. F. Scinocca and N. A. McFarlane. (2000) The parametrization of drag induced by stratified

1993 flow over anisotropic orography. *Quarterly Journal of the Royal Meteorological Society*

1994 **126**:568, 2353-2393.

1995

1996 Scinocca, J. F., McFarlane, N. A. Lazare, M., Li, J., and Plummer, D.: Technical Note: The  
1997 CCCma third generation AGCM and its extension into the middle atmosphere, *Atmos. Chem.*  
1998 *Phys.*, 8, 7055–7074, doi:10.5194/acp-8-7055-2008, 2008.  
1999  
2000 Scorer, R. S., 1949: Theory of waves in the lee of mountains. *Q. Jour. Royal Met. Soc.*, 75, 41-  
2001 56  
2002  
2003 Serva F., C. Cagnazzo, A. Riccio and E. Manzini, Impact of a Stochastic Nonorographic Gravity  
2004 Wave Parameterization on the Stratospheric Dynamics of a General Circulation Model, *Journal*  
2005 *of Advances in Modeling Earth Systems*, 10, 9, (2147-2162), (2018).  
2006  
2007 Sheppard P. A. (1956) Airflow over mountains. *Q J R Meteorol Soc*, 82, 528–529  
2008  
2009 Smith R. B.,, 1979: The influence of mountains on the atmosphere. *Advances in Geophysics*, B.  
2010 Saltzman, Ed., Vol. 21, Academic Press, 87–230, [https://doi.org/10.1016/S0065-2687\(08\)60262-](https://doi.org/10.1016/S0065-2687(08)60262-9)  
2011 [9](https://doi.org/10.1016/S0065-2687(08)60262-9)  
2012  
2013 Smith, R. B., 1980: Linear theory of stratified hydrostatic flow past an isolated mountain. *Tellus*,  
2014 **32**, 348–364.  
2015  
2016 Smith, R.B., 1985: On Severe Downslope Winds. *J. Atmos. Sci.*, **42**, 2597–2603,  
2017 [https://doi.org/10.1175/1520-0469\(1985\)042<2597:OSDW>2.0.CO;2](https://doi.org/10.1175/1520-0469(1985)042<2597:OSDW>2.0.CO;2)  
2018  
2019 Smith, R. B., 1989: Hydrostatic airflow over mountains. *Adv. Geophys.*, 31, 1- 41  
2020  
2021 Smith, A. K., and G. P. Brasseur (1991), Numerical simulation of the seasonal variation of  
2022 mesospheric water vapor, *J. Geophys. Res.*, 96, 7553–7563, doi:10.1029/91JD00226.  
2023  
2024 Smith R. B., and C. G. Kruse, 2017: Broad-spectrum mountain waves. *J. Atmos. Sci.*, 74, 1381–  
2025 1402, <https://doi.org/10.1175/JAS-D-16-0297.1>.  
2026  
2027 Smolarkiewicz, P. K., and R. Rotunno, 1990: Low Froude number flow past three-dimensional  
2028 obstacles. Part II: Upwind flow reversal zone. *J. Atmos. Sci.*, 47, 1498–1511.  
2029  
2030 Smith, R.B., A.D. Nugent, C.G. Kruse, D.C. Fritts, J.D. Doyle, S.D. Eckermann, M.J. Taylor, A.  
2031 Dörnbrack, M. Uddstrom, W. Cooper, P. Romashkin, J. Jensen, and S. Beaton, 2016:  
2032 Stratospheric Gravity Wave Fluxes and Scales during DEEPWAVE. *J. Atmos. Sci.*, **73**, 2851–  
2033 2869, <https://doi.org/10.1175/JAS-D-15-0324.1>  
2034  
2035 Smith, R.B. and C.G. Kruse, 2017: Broad-Spectrum Mountain Waves. *J. Atmos. Sci.*, **74**, 1381–  
2036 1402, <https://doi.org/10.1175/JAS-D-16-0297.1>  
2037  
2038 Smith, R.B. and C.G. Kruse, 2018: A Gravity Wave Drag Matrix for Complex Terrain. *J. Atmos.*  
2039 *Sci.*, **75**, 2599–2613, <https://doi.org/10.1175/JAS-D-17-0380.1>  
2040

2041 Smith, R. B., 2019: 100 years of progress on mountain meteorology research. Book chapter  
2042 under review.

2043

2044 Snively, J. B., and V. P. Pasko (2008), Excitation of ducted gravity waves in the lower  
2045 thermosphere by tropospheric sources, *J. Geophys. Res.*,  
2046 *113*, A06303, doi:10.1029/2007JA012693.

2047

2048 Song, I.-S., H.-Y. Chun, and T. P. Lane, 2003: Generation mechanisms of convectively forced  
2049 internal gravity waves and their propagation to the stratosphere. *J. Atmos. Sci.*, **60**, 1960–1980,  
2050 doi:[https://doi.org/10.1175/1520-0469\(2003\)060<1960:GMOCFI>2.0.CO;2](https://doi.org/10.1175/1520-0469(2003)060<1960:GMOCFI>2.0.CO;2).

2051

2052 Song I-S. and H-Y. Chun (2005) Momentum Flux Spectrum of Convectively Forced Internal  
2053 Gravity Waves and Its Application to Gravity Wave Drag Parameterization. Part I: Theory.  
2054 *Journal of the Atmospheric Sciences* **62**:1, 107-124.

2055

2056 Song, I.-S., and H.-Y. Chun 2008: A Lagrangian spectral parameterization of gravity wave drag  
2057 induced by cumulus convection. *J. Atmos. Sci.*, **65**, 1204–1224.

2058

2059 Stephan, C., M.J. Alexander, and J.H. Richter, 2016: Characteristics of Gravity Waves from  
2060 Convection and Implications for Their Parameterization in Global Circulation Models. *J. Atmos.*  
2061 *Sci.*, **73**, 2729–2742, <https://doi.org/10.1175/JAS-D-15-0303.1>

2062

2063 Su, T., & Zhai, G. (2017). The role of convectively generated gravity waves on convective  
2064 initiation: A case study. *Monthly Weather Review*, *145*, 335–359.

2065

2066 Sugimoto, N., Ishioka, K., Ishii, K., 2008: Parameter sweep experiments on spontaneous gravity  
2067 wave radiation from unsteady rotational flow in an f-plane shallow water system. *J. Atmos.*  
2068 *Sci.* **65**, 235–249.

2069

2070 Tabaei, A., and T. R. Akylas, 2007: Resonant long-short wave interactions in an unbounded  
2071 rotating stratified fluid. *Stud. Appl. Math.*, **119**, 271–296. Uccellini, L., and S. Koch (1987), The  
2072 synoptic setting and possible energy sources for mesoscale wave disturbances, *Mon. Weather*  
2073 *Rev.*, *115*, 721–729.

2074

2075 Teixeira, M. A. C., 2014: The physics of orographic gravity wave drag. *Frontiers in Physics*,  
2076 <https://doi.org/10.3389/fphy.2014.00043>

2077

2078 Vadas, S. L., D. C. Fritts, and M. J. Alexander(2003), Mechanism for the generation of secondary  
2079 waves in wave breaking regions, *J. Atmos. Sci.*, **60**, 194–214.

2080

2081 Vadas, S.L., J. Zhao, X. Chu and E. Becker, 2018, "The Excitation of secondary gravity waves  
2082 from local body forces: Theory and observation", *J. Geophys. Res. Atmospheres*, **123**,  
2083 <https://doi.org/10.1029/2017JD027970>.

2084

2085 Vadas, S.L., H.-L. Liu, and R.S. Lieberman, 2014, "Numerical modeling of the global changes to  
2086 the thermosphere and ionosphere from the dissipation of gravity waves from deep convection",  
2087 JGR Space Physics, 119, doi:10.1002/2014JA020280  
2088

2089 Vadas, S.L., J. Zhao, X. Chu and E. Becker, 2018, "The Excitation of secondary gravity waves  
2090 from local body forces: Theory and observation", J. Geophys. Res. Atmospheres, 123,  
2091 <https://doi.org/10.1029/2017JD027970>.  
2092

2093 Vadas, S. L. and M. J. Nicolls, 2012, "The Phases and Amplitudes of Gravity Waves  
2094 Propagating and Dissipating in the Thermosphere: Theory", J. Geophys. Res, 117, A05322,  
2095 doi:10.1029/2011JA017426.  
2096

2097 Vadas, S. L., and D. C. Fritts, 2005: "Thermospheric responses to gravity waves: Influences of  
2098 increasing viscosity and thermal diffusivity", J. Geophys. Res., 110,  
2099 D15103} {doi:10.1029/2004JD005574}.

2100

2101 Vadas, S. L. 2007: "Horizontal and vertical propagation, and dissipation of gravity waves in the  
2102 thermosphere from lower atmospheric and thermospheric sources", J. Geophys. Res.,  
2103 {112}'{A06305, doi:10.1029/2006JA011845}.

2104

2105 Vadas, S. L., and M. J. Nicolls (2012), The phases and amplitudes of gravity waves propagating  
2106 and dissipating in the thermosphere: Theory, J. Geophys. Res., 117, A05322,  
2107 doi:10.1029/2011JA017426.  
2108

2109 Van den Bremer, T. S., and B. R. Sutherland, 2014: The mean flow and long waves induced by  
2110 two-dimensional internal gravity wavepackets. Phys. Fluids, 26 (10), 106601, doi:10.1063/1.  
2111 4899262.  
2112

2113 Vanneste, J. (2008), Exponential smallness of inertia-gravity-wave generation at small rossby  
2114 number, *J. Atmos. Sci.*, 65, 1622–1637.  
2115

2116 Vanneste, J., and I. Yavneh (2004), Exponentially small inertia-gravity waves and the  
2117 breakdown of quasi-geostrophic balance, *J. Atmos.*  
2118 *Sci.*, 61, 211–223.  
2119

2120 Vincent, R. A., S. J. Allen, and S. D. Eckermann, 1997: Gravity wave parameters in the lower  
2121 stratosphere. Gravity Wave Processes: Their Parameterization in Global Climate Models, K.  
2122 Hamilton, Ed., Springer, 7–25.

2123 Wang, J., Kim, H.-M., & Chang, E. K. M. (2018). Interannual modulation of Northern  
2124 Hemisphere winter storm tracks by the QBO. *Geophysical Research Letters*, 45.  
2125 <https://doi.org/10.1002/2017GL076929>

2126 Walterscheid, R. L., and M. P. Hickey (2011), Group velocity and energy flux in the  
2127 thermosphere: Limits on the validity of group velocity in a viscous atmosphere, *J. Geophys. Res.*,  
2128 116, D12101, doi: 10.1029/2010JD014987.  
2129



2130 Wang, J., H.-M. Kim, E. K. M. Chang, and S.-W. Son, 2018: Modulation of the MJO and North  
2131 Pacific storm track relationship by the QBO. *J. Geophys. Res. Atmos.*, 123, 3976– 3992,  
2132 <https://doi.org/10.1029/2017JD027977>.  
2133

2134 Wang, L., and M. Geller (2003), Morphology of gravity-wave energy as observed from 4 years  
2135 (1998–2001) of high vertical resolution U.S.  
2136 radiosonde data, *J. Geophys. Res.*, 108, 4489, doi:10.1029/2002JD002786.  
2137

2138 Warner, C. D., and M. E. McIntyre, An ultra-simple spectral parameterization for non-  
2139 orographic gravity waves, *J. Atmos. Sci.*, 58, 1837–1857, 2001  
2140

2141 Webster, S., A. R. Brown, D. R. Cameron, and C. P. Jones, 2003: Improvements to the  
2142 representation of orography in the Met Office Unified Model. *Quart. J. Roy. Meteor. Soc.*, 129,  
2143 1989– 2010, <https://doi.org/10.1256/qj.02.133>.  
2144

2145 Wei, J., and F. Zhang, 2014: Mesoscale gravity waves in moist baroclinic jet–front systems. *J.*  
2146 *Atmos. Sci.*, 71, 929–952, doi:10.1175/JAS-D-13-0171.1.  
2147

2148 Wei, J., and F. Zhang, 2015: Tracking gravity waves in moist baroclinic jet-front systems. *J.*  
2149 *Adv. Model. Earth Syst.*, 7, 67-91, doi: 10.1002/2014MS000395  
2150

2151 Wei, J., F. Zhang, and J. H. Richter, 2016: An analysis of gravity wave spectral characteristics in  
2152 moist baroclinic jet-front systems. *J. Atmos. Sci.*, 73, 3133–3155, doi:10.1175/JAS-D-15-0316.1.  
2153

2154 Wei, J., G. Bölöni, and U. Achatz, 2019: Efficient modelling of the interaction of mesoscale  
2155 gravity waves with unbalanced large-scale flows: Pseudomomentum-flux convergence versus  
2156 direct approach. *J. Atmos. Sci.*, 76, 2715-2738, doi: <https://doi.org/10.1175/JAS-D-18-0337.1>  
2157

2158 Wilhelm, J., T. R. Akylas, G. Bölöni, J. Wei, B. Ribstein, R. Klein, and U. Achatz, 2017:  
2159 Interactions between Mesoscale and Submesoscale Gravity Waves and Their Efficient  
2160 Representation in Mesoscale-Resolving Models. *J. Atmos. Sci.*, 75, 2257-2280, doi:  
2161 <https://doi.org/10.1175/JAS-D-17-0289.1>  
2162

2163 Winters, K., & Armi, L. (2014). Topographic control of stratified flows: Upstream jets, blocking  
2164 and isolating layers. *Journal of Fluid Mechanics*, 753, 80-103. doi:10.1017/jfm.2014.363  
2165

2166 Wu, D. L., and F. Zhang, 2004: A study of mesoscale gravity waves over the North Atlantic with  
2167 satellite observations and a mesoscale model. *J. Geophys. Res.*, 109, D22104, doi:10.1029/  
2168 2004JD005090.  
2169

2170 Yiğit, E., A. S. Medvedev, A. D. Aylward, P. Hartogh, and M. J. Harris (2009), Modeling the  
2171 effects of gravity wave momentum deposition on the general circulation above the turbopause, *J.*  
2172 *Geophys. Res.*, 114, D07101, doi: 10.1029/2008JD011132.  
2173

2174 Yiğit, E., and A. S. Medvedev (2009), Heating and cooling of the thermosphere by internal  
2175 gravity waves, *Geophys. Res. Lett.*, 36, L14807, doi: 10.1029/2009GL038507.



2176 Yoo, C., and S.-W. Son (2016), Modulation of the boreal wintertime Madden-Julian oscillation  
2177 by the stratospheric quasi-biennial oscillation, *Geophys. Res. Lett.*, 43, 1392–1398,  
2178 doi:10.1002/2016GL067762.

2179 Yu, Y., W. Wang and M. P. Hickey (2017), Ionospheric signatures of gravity waves produced by  
2180 the 2004 Sumatra and 2011 Tohoku tsunamis: A modeling study, *J. Geophys. Res. Space*  
2181 *Physics*, 121, doi:10.1002/2016JA023116.

2182  
2183 Su T. and Guoqing Zhai. (2017) The Role of Convectively Generated Gravity Waves on  
2184 Convective Initiation: A Case Study. *Monthly Weather Review* **145**:1, 335-359.

2185  
2186 Zhang, F., 2004: Generation of mesoscale gravity waves in the upper- tropospheric jet-front  
2187 systems. *J. Atmos. Sci.*, 61, 440–457.

2188  
2189 Zhang, D.-L., and J. Fritsch (1988), Numerical simulation of the meso-b scale structure and  
2190 evolution of the 1977 Johnstown flood. Part III: Internal gravity waves and the squall line, *J.*  
2191 *Atmos. Sci.*, 45, 1252–1268.

2192  
2193 Zhang, F., and S. Koch (2000), Numerical simulations of a gravity wave event over CCOPE.  
2194 Part II: Waves generated by an orographic density current, *Mon. Weather Rev.*, 128(8), 2777–  
2195 2796.

2196  
2197 Zhang, F., S. Koch, C. Davis, and M. Kaplan (2001), Wavelet analysis and the governing  
2198 dynamics of a large amplitude mesoscale gravity wave event along the east coast of the united  
2199 states, *Q. J. R. Meteorol. Soc.*, 127, 2209–2245.

2200  
2201 Zhang, F., S. Koch, and M. Kaplan (2003), Numerical simulations of a large-amplitude gravity  
2202 wave event, *Meteo. Atmos. Phys.*, 84, 199–216.

2203  
2204 Zhang, S., and F. Yi (2005), A statistical study of gravity waves from radiosonde observations at  
2205 Wuhan (30 degrees N, 114 degrees E) China, *Ann. Geophys.*, 23, 665–673.

2206  
2207 Zhang, S., and F. Yi (2008), Intensive radiosonde observations of gravity waves in the lower  
2208 atmosphere over Yichang (111 degrees 18' E, 30 degrees 42' N), China, *Ann. Geophys.*, 26(7),  
2209 2005–2018.

2210  
2211  
2212  
2213